IMA Journal of Numerical Analysis (2017) **00**, 1–36
doi: 10.1093/imanum/drx058

Preserving invariance properties of reaction–diffusion systems on stationary surfaces

MASSIMO FRITTELLI*
Dipartimento di Matematica e Fisica "E. De Giorgi", Università del Salento, via per Arnesano, I-73100 Lecce, Italy
*Corresponding author: massimo.frittelli@unisalento.it

ANOTIDA MADZVAMUSE
Department of Mathematics, School of Mathematical and Physical Sciences, University of Sussex, Brighton, BN1 9QH, UK
A.Madzvamuse@sussex.ac.uk

IVONNE SGURA
Dipartimento di Matematica e Fisica "E. De Giorgi", Università del Salento, via per Arnesano, I-73100 Lecce, Italy
ivonne.sgura@unisalento.it

AND

CHANDRASEKHAR VENKATARAMAN
School of Mathematics and Statistics, University of St Andrews, Fife, KY16 9SS, UK
cv28@st-andrews.ac.uk

[Received on 14 February 2017; revised on 18 July 2017]

We propose and analyse a lumped surface finite element method for the numerical approximation of reaction–diffusion systems on stationary compact surfaces in $\mathbb{R}^3$. The proposed method preserves the invariant regions of the continuous problem under discretization and, in the special case of scalar equations, it preserves the maximum principle. On the application of a fully discrete scheme using the implicit–explicit Euler method in time, we prove that invariant regions of the continuous problem are preserved (i) at the spatially discrete level with no restriction on the meshsize and (ii) at the fully discrete level under a timestep restriction. We further prove optimal error bounds for the semidiscrete and fully discrete methods, that is, the convergence rates are quadratic in the meshsize and linear in the timestep. Numerical experiments are provided to support the theoretical findings. We provide examples in which, in the absence of lumping, the numerical solution violates the invariant region leading to blow-up.

Keywords: surface finite elements; mass lumping; invariant region; maximum principle; reaction–diffusion; heat equation; convergence; pattern formation.

1. Introduction

Partial differential equations (PDEs) of the form of reaction–diffusion systems (RDSs) have been extensively employed to model many different processes in a wide range of fields such as biology (Murray, 2001; Ferreira *et al.*, 2002; Nijhout *et al.*, 2003), chemistry (Vanag, 2004), electrochemistry (Bessler, 2005; Lacitignola *et al.*, 2015) and finance (for example, Becherer & Schweizer, 2005). In many applications, the domain of integration is a stationary or an evolving curved surface, rather than a planar region. For instance, surface RDSs have been applied to the study of biological patterning (Barreira *et al.*, 2011),

tumour growth (Chaplain *et al.*, 2001), metal dealloying (Eilks & Elliott, 2008), biomembrane modelling (Elliott & Stinner, 2010), electrochemistry (Lacitignola *et al.*, 2017) and cell motility (Elliott *et al.*, 2012), just to mention a few examples. In this article, we consider RDSs of arbitrarily many equations on a stationary surface of the form

$$\begin{cases} \dfrac{\partial u_k}{\partial t} - d_k \Delta_\Gamma u_k = f_k(u_1, \dots, u_r), \qquad k = 1, \dots, r, \qquad \text{in } \Gamma \times (0, T], \\ u_k(\mathbf{x}, 0) = u_{0k}(\mathbf{x}) \qquad \forall\, \mathbf{x} \in \Gamma, \end{cases} \tag{1.1}$$

where Γ is a smooth stationary orientable surface of codimension 1 in $\mathbb{R}^3$ without boundary, Δ_Γ is the Laplace–Beltrami operator on Γ (which is defined as the tangential divergence of the tangential gradient; see Dziuk & Elliott, 2013a for the definitions), each d_k is a strictly positive diffusion coefficient, while the regularity of the kinetics and the initial data are such that a unique solution to (1.1) exists (see, for example, Taylor, 1997, Chapter 15.1). Precise assumptions are given in Section 3.1.

The increasing interest from applications in RDSs on manifolds has stimulated the development of several numerical methods for such systems. Among the methods for PDEs on stationary surfaces we recall finite differences (Varea *et al.*, 1999), the spectral method of lines (Chaplain *et al.*, 2001), closest point methods (see Macdonald & Ruuth, 2009 and references therein), kernel methods (see Shankar *et al.*, 2015 and references therein), embedding methods (see Bertalmío *et al.*, 2003), surface finite element methods (SFEM) and their extensions (see Dziuk, 1988; Olshanskii *et al.*, 2009; Dziuk & Elliott, 2013a; Burman *et al.*, 2015; Tuncer *et al.*, 2015). In this article, we consider a lumped mass surface finite element method (LSFEM) for the spatial discretization of Eqs. (1.1). We recall that finite elements with mass lumping have already been applied to RDSs on planar domains (see, for example, Nie & Thomée, 1985; Elliott & Stuart, 1993; Garvie & Trenchea, 2007; Chatzipantelidis *et al.*, 2015) and to bulk–surface parabolic problems (see Kovács & Lubich, 2016).

A standard approach for carrying out a fully discrete scheme is the implicit–explicit (IMEX) method that treats diffusion implicitly and reactions explicitly. IMEX methods have been widely applied in fluid dynamics, combined with spectral methods on planar domains (Kim & Moin, 1985; Canuto *et al.*, 2012), in reaction–diffusion problems, in combination with finite differences in space on planar domains (Ruuth, 1995), with finite elements on stationary planar domains (Elliott & Stuart, 1993), on evolving planar domains (Madzvamuse, 2006) and with the closest point method on stationary surfaces (Macdonald, 2008). An error analysis of finite element approximations with IMEX timestepping for semilinear systems on evolving domains is carried out in Lakkis *et al.* (2013). Among IMEX methods, we will consider the simplest one: the IMEX Euler scheme considered, for example, in Madzvamuse (2006) and Lakkis *et al.* (2013).

A key feature of many RDSs is the existence of invariant regions. A region Σ in the phase space $\mathbb{R}^r$ is said to be invariant for (1.1) if, whenever the initial condition has values in Σ, the solution of (1.1) stays in Σ as long as it is defined. Knowing that a given model possesses an invariant region is useful in a couple of ways. First, when solving RDSs arising from applications, solutions are usually meaningful as long as they range within a limited set of values (for example, in some cases they must be between 0 and 1 to remain physically meaningful, as in Lacitignola *et al.*, 2015). Second, an invariant region provides an *a priori* bound on the analytical solution that can be helpful, for instance, when studying the convergence of numerical methods. Sufficient conditions for a region to be invariant for a given RDS were given in Chueh *et al.* (1977) and Smoller (1994) on planar domains and in Taylor (1997, pp. 335–353) on stationary surfaces. In both cases, for distinct d_k's, the only possible invariant regions for (1.1) are

(bounded or unbounded) hyperrectangles in $\mathbb{R}^r$ of the form

$$\Sigma = \prod_{k=1}^{r} [m_k, M_k], \tag{1.2}$$

with $m_k \in \mathbb{R} \cup \{-\infty\}$ and $M_k \in \mathbb{R} \cup \{+\infty\}$ for all $k = 1, \ldots, r$, whereas if some d_k coincide, more general regions are allowed to be invariant. Since we are addressing general diffusion coefficients, we will consider invariant hyperrectangles (1.2) only. Among the literature on RD models having invariant hyperrectangles, we recall the Gierer–Meinhardt (Kovács, 2003), Hodgkin–Huxley (Galusinski, 1998), FitzHugh–Nagumo (Rauch & Smoller, 1978), Oregonator (You, 2012), Rosenzweig–MacArthur (Skalski & Gilliam, 2001; González-Olivares & Ramos-Jiliberto, 2003) and the spatially extended Lotka–Volterra models (Alikakos, 1979). For $r = 1$ in (1.1), i.e., scalar semilinear equations, we remark that the min-max condition and the maximum principle, given, respectively, by

$$\min_{\Gamma} u_0 \leq u(\mathbf{x}, t) \leq \max_{\Gamma} u_0 \quad \text{and} \quad 0 \leq u(\mathbf{x}, t) \leq \max_{\Gamma} u_0 \qquad \forall\, (\mathbf{x}, t) \in \Gamma \times [0, T], \tag{1.3}$$

can be regarded in terms of invariant regions. In fact, conditions (1.3) correspond to the invariance of the following families of invariant regions: $[m, M]$ for all $m, M \in \mathbb{R}$, $m < M$ and $[0, M]$ for all $M > 0$.

When numerically approximating RDSs, it is desirable for the considered numerical method to preserve invariant rectangles of the continuous problem. In the case of stationary or evolving surfaces, to the best of our knowledge, only a time-dependent discrete maximum principle for the heat equation is given in the recent work by Kovács *et al.* (2017), in which the evolving surface finite element method (ESFEM) is applied. In the case of stationary planar domains, RDSs of many equations have been considered in Hoff (1978), in which the spatial discretization is carried out through finite differences, and the invariant rectangles are preserved under meshsize restrictions. The more recent work by Garvie & Trenchea (2007) considers the lumped finite element method (LFEM) for particular RDSs and proves the preservation of the positive quadrant by using globally positive modified kinetics.

More studied is the scalar case on stationary planar domains. We recall once again that, for scalar equations, the maximum principle can be regarded in terms of invariant regions. Work in this direction is that of Faragó *et al.* (2012), which considers the standard FEM and proves a discrete maximum principle under a meshsize restriction. Such restrictions can be avoided by applying the LFEM (see Nie & Thomée, 1985; Elliott & Stuart, 1993; Chatzipantelidis *et al.*, 2015 and references therein).

To the best of our knowledge, numerical methods for surface RDSs that preserve the invariant rectangles of the continuous problem have not yet been investigated. This motivates the present study in which we introduce the LSFEM, which not only preserves the invariant rectangles of surface RDSs at the discrete level but also requires no restriction on the meshsize and no modification to the kinetics.

The main contributions of this article are the following:

1. For RDSs of the form (1.1), we prove that the LSFEM and the IMEX Euler-LSFEM preserve the invariant rectangles. A timestep restriction depending on the Lipschitz constants of the kinetics is needed at the fully discrete level. These preservation results, which require no space meshsize restriction or modified kinetics, are novel even in the specific case of planar domains.
2. A consequence of invariant region preservation is stability. In the literature, when the preservation results are not available, more sophisticated techniques are adopted for guaranteeing stability, for instance, a globally Lipschitz extension of the kinetics outside the invariant region (see

Lakkis *et al.*, 2013). The drawback of Lipschitz extensions is that they are not always computable. Therefore, once again the method we propose in this work is fully practical as it does not need any meshsize restriction nor modified kinetics. The importance of invariant-region preservation in terms of stability is also shown in two numerical tests: numerical experiment 2 for the scalar case and numerical experiment 3 for system (1.1). To demonstrate the applicability of our numerical method, we consider the Rosenzweig–MacArthur kinetics on a Dupin ring cyclide, which possesses a bounded invariant rectangle, in which the SFEM solution blows up, while the LSFEM solution remains in the invariant rectangle.

3. By exploiting the stability estimates arising from invariant-region preservation, we prove optimal error bounds for the semidiscrete and fully discrete schemes. These results are novel in that they account for errors arising from mass lumping and surface approximation, respectively. Two numerical examples on the unit sphere confirm the result (i) for the linear heat equation (numerical experiment 1) and (ii) for the Schnakenberg RD model (numerical experiment 4).

The remainder of the present article is structured as follows. In Section 2, we consider a semilinear scalar parabolic equation on a closed orientable surface in strong and weak formulation. We present its LSFEM space discretization, its Euler IMEX/L\SFEM full discretization and prove the preservation of the maximum principle under spatial and full discretization in Theorems 2.3 and 2.4, respectively. In Section 3, we consider a general RDS of arbitrarily many equations on closed orientable surfaces, we derive the LSFEM space discretization, its Euler IMEX/LSFEM time discretization and prove the preservation of invariant rectangles under spatial and full discretizations in Theorems 3.3 and 3.5, respectively. In Section 4, optimal error estimates for both the semidiscrete and fully discrete methods introduced in the previous sections are proved in Theorems 4.8 and 4.9, respectively. Numerical experiments are shown in Section 5.

2. A semilinear scalar parabolic equation

2.1 *The continuous problem*

We start by considering scalar parabolic PDEs to illustrate the main ideas behind the approach described in this work and to introduce the analysis in a less technical setting.

Let Γ be a compact, orientable, smooth surface of codimension 1 in $\mathbb{R}^3$ without boundary. We assume that Γ is represented as the zero level set of a sufficiently smooth *signed distance function* d, defined in an open neighbourhood W of Γ such that $\nabla d(\mathbf{x}) \neq \mathbf{0}$ for all $\mathbf{x} \in W$ by

$$\Gamma = \{\mathbf{x} \in W \mid d(\mathbf{x}) = 0\}.$$

The normal unit vector on Γ is then defined by $\boldsymbol{\nu}(\mathbf{x}) = \frac{\nabla d(\mathbf{x})}{|\nabla d(\mathbf{x})|}$ for all $\mathbf{x} \in \Gamma$. We assume that every point $\mathbf{x} \in W$ may be uniquely represented as

$$\mathbf{x} = \mathbf{a}(\mathbf{x}) + d(\mathbf{x})\boldsymbol{\nu}(\mathbf{a}(\mathbf{x})), \tag{2.1}$$

with $\mathbf{a}(\mathbf{x}) \in \Gamma$. A sufficient condition on the thickness of W such that this property holds (in this case W is called a *Fermi stripe*) is given in Dziuk & Elliott (2013a).

We briefly recall the definitions of Sobolev and Bochner spaces on surfaces. For $q \in \mathbb{N} \cup \{0\}$, the Sobolev space $H^q(\Gamma)$ is the space of functions $u : \Gamma \to \mathbb{R}$ such that, for all $i = 0, \ldots, q$, the ith-order

tangential derivatives, meant in a distributional sense, are in $L^2(\Gamma)$, while $H^{-q}(\Gamma)$ is the dual space of $H^q(\Gamma)$, that is, the space of linear continuous functionals on $H^q(\Gamma)$. For $p \in [1, +\infty]$, if X is a Banach space, the Bochner space $L^p([0,T];X)$ is the space of functions $u : [0,T] \to X$ such that the function $\|u\|_X : [0,T] \to \mathbb{R}$ is $L^p([0,T])$. For further details on Sobolev and Bochner spaces on surfaces, we refer the interested reader to Taylor (1997), Hebey & Robert (2008) and Gilbarg & Trudinger (2015).

In this section, we consider the following semilinear parabolic equation posed on Γ defined as

$$\dot{u} - d\Delta_\Gamma u = -\beta u^\alpha, \qquad \mathbf{x} \in \Gamma,\ t \in (0,T], \tag{2.2}$$

where the dot denotes the time derivative, $d > 0$, $\alpha \geq 1$, $\beta \geq 0$, endowed with the non-negative $\mathcal{C}^2(\Gamma)$ initial condition

$$u(\mathbf{x},0) = u_0(\mathbf{x}), \qquad \mathbf{x} \in \Gamma.$$

The requirement that $\alpha \geq 1$ is needed to make sure that the source term u^α is Lipschitz in a neighbourhood of $u = 0$, which is a necessary condition for the existence and uniqueness of a solution at all positive times. The conditions $\beta \geq 0$ and $u_0 \geq 0$ together are needed to guarantee the maximum principle (1.3). The homogeneous heat equation is obtained as a special case for $\beta = 0$. The weak formulation of the problem seeks to find $u \in L^2([0,T];H^1(\Gamma)) \cap L^\infty([0,T] \times \Gamma)$ with $\dot{u} \in L^2([0,T];H^{-1}(\Gamma))$ such that

$$\int_\Gamma \dot{u}\varphi + d\int_\Gamma \nabla_\Gamma u \cdot \nabla_\Gamma \varphi = -\beta \int_\Gamma u^\alpha \varphi, \qquad \forall\, \varphi \in H^1(\Gamma). \tag{2.3}$$

2.2 *Space discretization*

As mentioned previously, in the present work our focus is on finite element discretizations. We now present the necessary notation and concepts needed to describe the numerical method.

Given $h > 0$, a triangulated surface $\Gamma_h \subset W$ is defined by

$$\Gamma_h = \bigcup_{K \in \mathcal{K}_h} K,$$

where $\mathcal{K}_h$ is a set of finitely many non overlapping, nondegenerate triangles, whose diameters do not exceed h and whose vertices $\{\mathbf{x}_i\}_{i=1}^N$ lie on Γ, such that, for $\mathbf{a}(\mathbf{x})$ as defined in (2.1), $\mathbf{a}_{|\Gamma_h}(\mathbf{x})$ is a one-to-one map between Γ and $\Gamma_h \subset W$.

Following Dziuk & Elliott (2013a), we define lifts and unlifts in order to compare functions on the triangulated and smooth surfaces. Let $\mathbf{a}(\cdot)$ be as in (2.1), given a function $V : \Gamma_h \to \mathbb{R}$, its *lift* $V^\ell : \Gamma \to \mathbb{R}$ is defined by

$$V^\ell(\mathbf{a}(\mathbf{x})) = V(\mathbf{x}), \qquad \forall \mathbf{x} \in \Gamma_h.$$

Given a function $w : \Gamma \to \mathbb{R}$, its *unlift* $w^{-\ell} : \Gamma_h \to \mathbb{R}$ is defined by

$$w^{-\ell}(\mathbf{x}) = w(\mathbf{a}(\mathbf{x})), \qquad \forall\, \mathbf{x} \in \Gamma_h.$$

Next, let S_h be the space of piecewise linear functions on Γ_h defined by

$$S_h = \left\{ V \in \mathcal{C}^0(\Gamma_h) \mid V_{|K} \text{ is linear affine } \forall\, K \in \mathcal{K}_h \right\}$$

and S_h^ℓ be its lifted counterpart $S_h^\ell = \left\{V^\ell \mid V \in S_h\right\}$. Let $\{\chi_i\}_{i=1}^N$ be the nodal basis of S_h defined by

$$\chi_i(\mathbf{x}_j) = \delta_{ij} \qquad \forall\, i,j = 1,\dots,N. \tag{2.4}$$

For $w \in \mathcal{C}^0(\Gamma_h)$, the piecewise linear interpolant $I_h(w)$ of w is the function in S_h given by

$$I_h(w) = \sum_{i=1}^{N} w(\mathbf{x}_i)\chi_i. \tag{2.5}$$

We define the following semidiscrete problem: find $U \in L^2([0,T];S_h)$ with $\dot{U} \in L^2([0,T];S_h)$ such that

$$\int_{\Gamma_h} I_h(\dot{U}\phi) + d\int_{\Gamma_h} \nabla_{\Gamma_h} U \cdot \nabla_{\Gamma_h}\phi = -\beta \int_{\Gamma_h} I_h(U^\alpha \phi), \qquad \forall\, \phi \in S_h, \tag{2.6}$$

where the initial condition $U_0(\mathbf{x})$ is the piecewise linear interpolant $I_h(u_0^{-\ell})(\mathbf{x})$ of the unlifted exact initial condition $u_0(\mathbf{x})$. We express the semidiscrete solution U in terms of the nodal basis (2.4) as

$$U(\mathbf{x},t) = \sum_{i=1}^{N} \xi_i(t)\chi_i(\mathbf{x}) \qquad \text{with} \qquad \xi_i(0) = u_0(\mathbf{x}_i), \quad i = 1,\dots,N. \tag{2.7}$$

We then define the lumped mass matrix $\bar{M} = (\bar{m}_{ij})$ and the stiffness matrix $A = (a_{ij})$, respectively, by

$$\bar{m}_{ij} = \int_{\Gamma_h} I_h(\chi_i\chi_j) \qquad \forall\, i,j = 1,\dots,N, \tag{2.8}$$

$$a_{ij} = \int_{\Gamma_h} \nabla_{\Gamma_h}\chi_i \cdot \nabla_{\Gamma_h}\chi_j \qquad \forall\, i,j = 1,\dots,N. \tag{2.9}$$

We recall that the mass matrix used in the standard SFEM (see Dziuk, 1988; Dziuk & Elliott, 2013a) is defined by $m_{ij} = \int_{\Gamma_h} \chi_i\chi_j$ for all $i, j = 1,\dots,N$. Using the above notation, the semidiscrete problem (2.6) can be expressed as the following system of ordinary differential equations:

$$\bar{M}\dot{\boldsymbol{\xi}} + dA\boldsymbol{\xi} = -\beta\bar{M}\boldsymbol{\xi}^\alpha, \tag{2.10}$$

where $\boldsymbol{\xi} := (\xi_1,\dots,\xi_N)^{\mathrm{T}}$.

2.2.1 *Mesh regularity.* In the following we will show that, under suitable assumptions on the triangulation $\mathcal{K}_h$, the LSFEM fulfils a discrete maximum principle, that is, the discrete version of (1.3). To this end, we introduce a regularity assumption for the triangulation on the mesh $\mathcal{K}_h$ that mimicks the standard Delaunay condition on planar domains and then we show how it affects the properties of the stiffness matrix A in (2.9).

Let e be an edge of the triangulation $\mathcal{K}_h$ and let K_1 and K_2 be the triangles sharing the edge e. Let α_1 and α_2 be the angles in K_1 and K_2 , respectively. that are opposite to e. For every edge e in $\mathcal{K}_h$, we require that

$$\alpha_1 + \alpha_2 \le \pi. \tag{2.11}$$

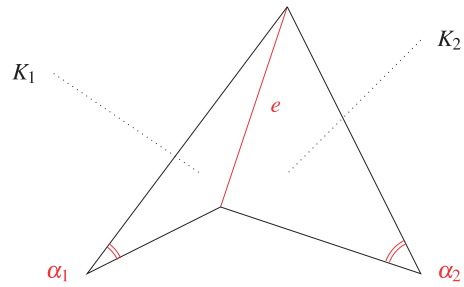

FIG. 1. Schematic representation of condition (2.11) for triangles K_1 and K_2.

This condition is represented in Fig. 1.

REMARK 2.1 We remark that the construction of good quality meshes on arbitrary surfaces is well studied in the literature and some theoretical works in this area are available (see, for instance, Persson, 2004; Dyer, 2010; Dassi, 2014 and references therein). However, to the best of our knowledge, the work in these references does not explicitly discuss the construction of surface meshes fulfilling the Delaunay property (2.11). As far as we know, algorithms for the construction of Delaunay triangulations on arbitrary smooth surfaces remain an open area of research.

The following result extends to triangulated surfaces a characterization of (2.11) given in Thomée (1984) for the planar case.

LEMMA 2.2 The triangulation $\mathcal{K}_h$ fulfils (2.11) if and only if

$$\left(\nabla_{\Gamma_h}\chi_i, \nabla_{\Gamma_h}\chi_j\right) \leq 0 \qquad \forall\, i \neq j. \tag{2.12}$$

Proof. Let $\mathbf{x}_i$ and $\mathbf{x}_j$ be two distinct nodes of $\mathcal{K}_h$. If $\mathbf{x}_i$ and $\mathbf{x}_j$ are not neighbours then $(\nabla_{\Gamma_h}\chi_i, \nabla_{\Gamma_h}\chi_j) = 0$. Otherwise, let e be the edge connecting $\mathbf{x}_i$ and $\mathbf{x}_j$. Since the intersection of the support of the pyramidal functions χ_i and χ_j is $K_1 \cup K_2$ (see Fig. 1) then we can write

$$(\nabla_{\Gamma_h}\chi_i, \nabla_{\Gamma_h}\chi_j) = (\nabla_{K_1}\chi_i, \nabla_{K_1}\chi_j) + (\nabla_{K_2}\chi_i, \nabla_{K_2}\chi_j). \tag{2.13}$$

Let T_1 and T_2 be two linear transformations that map K_1 and K_2, respectively, into two triangles K_1^0 and K_2^0 contained in the $x - y$ plane, and let J_1 and J_2 be the Jacobians of T_1 and T_2, respectively. Then, expression (2.13) can be written equivalently as

$$\int_{K_1^0} \left(J_1 \nabla_{K_1^0}\left(\chi_i \circ T_1^{-1}\right)\right) \cdot \left(J_1 \nabla_{K_1^0}\left(\chi_j \circ T_1^{-1}\right)\right) \det(J_1) + \int_{K_2^0} \left(J_2 \nabla_{K_2^0}\left(\chi_i \circ T_2^{-1}\right)\right) \cdot \left(J_2 \nabla_{K_2^0}\left(\chi_j \circ T_2^{-1}\right)\right) \det(J_2).$$

We choose T_1 and T_2 as direct isometries, that is, $\det(J_1) = \det(J_2) = 1$. Since $\nabla_{K_1^0}$ and $\nabla_{K_2^0}$ both collapse to the standard gradient ∇ in $\mathbb{R}^2$, the expression above becomes

$$\int_{K_1^0} \nabla\left(\chi_i \circ T_1^{-1}\right) \cdot \nabla\left(\chi_j \circ T_1^{-1}\right) + \int_{K_2^0} \nabla\left(\chi_i \circ T_2^{-1}\right) \cdot \nabla\left(\chi_j \circ T_2^{-1}\right).$$

It is known that (see Thomée, 1984) this expression depends only on the transformed angles $\alpha_1^0 = \alpha_1$, $\alpha_2^0 = \alpha_2$ and is given by $-\frac{\sin(\alpha_1+\alpha_2)}{4\sin(\alpha_1)\sin(\alpha_2)}$, which is nonpositive if and only if $\alpha_1 + \alpha_2 \leq \pi$. This completes the proof. □

Next, we proceed to state two key properties associated with the lumped mass and stiffness matrices to be used throughout the analysis. Let $\mathbf{1}$ and $\mathbf{0}$ be the vector of 1s and the null vector in $\mathbb{R}^N$, respectively. As shown in Thomée (1984, pp. 272–273), the structure (2.12) of the stiffness matrix, together with the diagonal structure (2.8) of the lumped mass matrix, implies that, for every $s > 0$, $\bar{M} + sA$ is an M-matrix. It then follows that

$$(\bar{M} + sA)^{-1}\bar{M} \geq \mathbf{0}, \tag{2.14}$$

meaning that this matrix has non-negative entries. If $\boldsymbol{\xi} = \mathbf{1}$, from (2.7) we have $U(\mathbf{x}, t) = 1$ for all $(\mathbf{x}, t) \in \Gamma_h \times [0, T]$, and thus $\nabla_{\Gamma_h} U(\mathbf{x}, t)$ vanishes, which yields $A\mathbf{1} = \mathbf{0}$. It therefore follows that

$$(\bar{M} + sA)^{-1}\bar{M}\mathbf{1} = \mathbf{1}. \tag{2.15}$$

We will show that (2.14) and (2.15) play a crucial role in the discrete maximum principle for the parabolic equation (2.2) and the preservation of invariant regions of RDSs (see Section 3).

2.3 *Time discretization*

By applying the IMEX Euler scheme (i.e., treating diffusion implicitly and the reactions explicitly), with timestep $\tau > 0$, to (2.10) we obtain the fully discrete scheme

$$\bar{M}\frac{\boldsymbol{\xi}^{n+1} - \boldsymbol{\xi}^n}{\tau} + dA\boldsymbol{\xi}^{n+1} = -\beta\bar{M}(\boldsymbol{\xi}^n)^\alpha, \qquad n = 0, \ldots, N_T, \tag{2.16}$$

with $N_T := \lfloor \frac{T}{\tau} \rfloor$ and $\boldsymbol{\xi}^0 = \boldsymbol{\xi}(0)$, where $\boldsymbol{\xi}(t)$ is defined in (2.7), or equivalently,

$$\boldsymbol{\xi}^{n+1} = (\bar{M} + d\tau A)^{-1}\bar{M}(\boldsymbol{\xi}^n - \tau\beta(\boldsymbol{\xi}^n)^\alpha), \qquad n = 0, \ldots, N_T. \tag{2.17}$$

We remark that, for $\beta = 0$ (i.e. the homogeneous heat equation), the timestepping scheme collapses to the standard implicit Euler method.

2.4 *Semidiscrete and fully discrete maximum principles*

It is known that the lumped FEM fulfils a discrete maximum principle for the homogeneous heat equation on planar domains (see Thomée, 1984). This result has been generalized to general diffusion problems in divergence form in Nie & Thomée (1985). The purpose of this section is to extend this result to equation (2.2), which includes as a special case the homogeneous heat equation on Γ.

THEOREM 2.3 (Maximum principle for (2.6)) Under the Delaunay condition (2.11), the nodal vector $\boldsymbol{\xi}(t)$ of the semidiscrete solution of (2.6) fulfils the maximum principle

$$0 \leq \xi_i(t) \leq \max_{j=1,\ldots,N} \xi_j(0), \qquad \forall\, i = 1, \ldots, N,\ \forall\, t > 0. \tag{2.18}$$

Proof. We rewrite (2.10) as

$$\dot{\boldsymbol{\xi}} + d\bar{M}^{-1}A\boldsymbol{\xi} = -\beta\boldsymbol{\xi}^{\alpha}. \tag{2.19}$$

Consider the auxiliary equation

$$\dot{\boldsymbol{\xi}} = -d\bar{M}^{-1}A\boldsymbol{\xi} - \beta|\boldsymbol{\xi}|^{\alpha}\mathrm{sign}(\boldsymbol{\xi}), \tag{2.20}$$

where $|\boldsymbol{\xi}|$ and $\mathrm{sign}(\boldsymbol{\xi})$ are the componentwise absolute value and the componentwise sign function of $\boldsymbol{\xi}$, respectively. If $\mu = \max_{j=1,\dots,N}\xi_j(0)$, it is sufficient to prove that the solution of the ODE system (2.19) does not escape the region $\Sigma = [0,\mu]^N$, i.e., we have to prove that, for every $\varepsilon > 0$, the solution of (2.20) does not leave the region $\bar{\Sigma} := [-\varepsilon,\mu]^N$. To this end, we have to prove that the vector field on the right-hand side of (2.20), computed on every $(N-1)$-dimensional face of $\bar{\Sigma}$, points toward the interior of $\bar{\Sigma}$. To this end, let $\boldsymbol{\xi}$ be a point on $\partial\bar{\Sigma}$. This means that there exists $i = 1,\dots,N$ such that $\xi_i \in \{-\varepsilon,\mu\}$. Suppose $\xi_i = \mu$; in the case $\xi_i = -\varepsilon$, the proof is analogous. Then

$$\xi_j \le \xi_i, \quad j \ne i. \tag{2.21}$$

All we have to prove is that $\dot{\xi}_i$ is negative. Hence, we prove that

1. $-|\xi_i|^{\alpha}\mathrm{sign}(\xi_i) = -|\mu|^{\alpha}\mathrm{sign}(\mu) < 0$ from (2.21);
2. the ith component of the vector $-d\bar{M}^{-1}A\boldsymbol{\xi}$ is nonpositive. In fact, since $\bar{M}$ is a diagonal matrix, this component is given by

$$-(d\bar{M}^{-1}A\boldsymbol{\xi})_i = -d\bar{m}_{ii}^{-1}\sum_{j=1}^{N}a_{ij}\xi_j. \tag{2.22}$$

We can split the sum on the right-hand side by isolating the $a_{ii}\xi_i$ term:

$$d\bar{m}_{ii}^{-1}\left(-a_{ii}\xi_i + \sum_{j\in\{1,\dots,N\}\setminus\{i\}}(-a_{ij})\xi_j\right). \tag{2.23}$$

Since $a_{ij} \le 0$ for $i \ne j$ from Lemma 2.2 and $\xi_j \le \xi_i$ for $j \ne i$ from (2.21), expression (2.23) is less than or equal to

$$d\bar{m}_{ii}^{-1}\xi_i\left(-a_{ii} + \sum_{j\in\{1,\dots,N\}\setminus\{i\}}(-a_{ij})\right) = -d\bar{m}_{ii}^{-1}\xi_i\sum_{j=1}^{N}a_{ij}. \tag{2.24}$$

From the definition of A, we have

$$-d\bar{m}_{ii}^{-1}\xi_i\sum_{j=1}^{N}a_{ij} = -d\bar{m}_{ii}^{-1}\xi_i\int_{\Gamma_h}\nabla_{\Gamma_h}\chi_i\cdot\nabla_{\Gamma_h}\sum_{j=1}^{N}\chi_i. \tag{2.25}$$

Since Γ_h has no boundary, $\sum_{j=1}^{N} \chi_i(\mathbf{x}) = 1$, $\mathbf{x} \in \Gamma_h$, and thus

$$\nabla_{\Gamma_h} \sum_{j=1}^{N} \chi_i(\mathbf{x}) = 0, \qquad \mathbf{x} \in \Gamma_h. \tag{2.26}$$

By combining (2.22)–(2.26), we finally have

$$-(d\bar{M}^{-1}A\boldsymbol{\xi})_i \leq 0. \tag{2.27}$$

The above points (1) and (2) imply the desired result that $\dot{\xi}_i$ is negative. This completes the proof. □

THEOREM 2.4 (Maximum principle for (2.17)) Under the Delaunay condition (2.11), the fully discrete solution $\boldsymbol{\xi}^n$ with initial data $\boldsymbol{\xi}^0$ of scheme (2.17) fulfils the maximum principle

$$0 \leq \xi_i^n \leq \max_{j=1,\ldots,N} \boldsymbol{\xi}_j(0), \qquad \forall\, i = 1, \ldots, N,\ \forall\, n \in \mathbb{N}, \tag{2.28}$$

if the timestep $\tau > 0$ satisfies

$$\beta\tau \leq \left(\max_{\mathbf{y} \in \Gamma_h} \left\{ U^0(\mathbf{y}) \right\} \right)^{1-\alpha}. \tag{2.29}$$

In particular, for $\beta = 0$, (2.28) holds with no restriction on τ.

Proof. From the matrix properties (2.14) and (2.15) we have, for every $\tau > 0$,

$$(\bar{M} + d\tau A)^{-1}\bar{M}\mathbf{1} = \mathbf{1}, \tag{2.30}$$

$$(\bar{M} + d\tau A)^{-1}\bar{M} \geq \mathbf{0}. \tag{2.31}$$

Let $n = 0, \ldots, N_T$. We assume by induction that $\boldsymbol{\xi}^n \geq \mathbf{0}$. We have to prove that

$$\max_{i=1,\ldots,N} \boldsymbol{\xi}_i^{n+1} \leq \max_{i=1,\ldots,N} \boldsymbol{\xi}_i^n, \tag{2.32}$$

$$\boldsymbol{\xi}^{n+1} \geq \mathbf{0}. \tag{2.33}$$

We first prove (2.32). Using (2.30) and (2.31) in scheme (2.17), we observe that

$$\begin{aligned} \max_{i=1,\ldots,N} \xi_i^{n+1} &= \max_{i=1,\ldots,N} \left((\bar{M} + d\tau A)^{-1}\bar{M} \left(\xi_i^n - \tau\beta(\xi_i^n)^\alpha \right) \right) \\ &\leq (\bar{M} + d\tau A)^{-1}\bar{M} \left(\mathbf{1} \max_{i=1,\ldots,N} \left(\xi_i^n - \tau\beta(\xi_i^n)^\alpha \right) \right) = \max_{i=1,\ldots,N} \left(\xi_i^n - \tau\beta(\xi_i^n)^\alpha \right), \end{aligned} \tag{2.34}$$

Hence, (2.32) holds if

$$\max_{i=1,\ldots,N} (\xi_i^n - \tau\beta(\xi_i^n)^\alpha) \leq \max_{i=1,\ldots,N} (\xi_i^n). \tag{2.35}$$

Since, from the inductive hypothesis, $\boldsymbol{\xi}^n \geq \mathbf{0}$, then (2.35) holds. We are left to prove (2.33). Using (2.31) in the scheme (2.17), (2.33) holds if

$$\boldsymbol{\xi}^n - \tau\beta(\boldsymbol{\xi}^n)^\alpha \geq 0. \tag{2.36}$$

Condition (2.36) holds if

$$\tau\beta \leq \min_{i=1,\dots,N}\left(\left(\xi_i^n\right)^{1-\alpha}\right) \leq \left(\max_{i=1,\dots,N}(\xi_i^n)\right)^{1-\alpha}. \tag{2.37}$$

We have proved that, for all $n = 0,\dots,N_T$, (2.37) implies (2.32) and (2.33). From (2.32), the most severe of the timestep restrictions in (2.37) is

$$\tau\beta \leq \left(\max_{i=1,\dots,N}(\xi_i^0)\right)^{1-\alpha} = \left(\max_{\mathbf{y}\in\Gamma_h}\left\{U^0(\mathbf{y})\right\}\right)^{1-\alpha}, \tag{2.38}$$

which completes the proof. □

3. RDSs on surfaces

In this section, we consider a more general class of surface PDEs that are RDSs of arbitrarily many equations. Analogously to the semilinear parabolic equation (2.2), we apply a lumped finite element space discretization and an IMEX Euler time discretization. We prove that the LSFEM preserves the invariant hyperrectangles for the semidiscrete and fully discrete problems. For the latter case, a timestep restriction is required.

3.1 *The continuous problem*

If Γ is a compact orientable surface in $\mathbb{R}^3$ without boundary, as in the previous section, and $r \in \mathbb{N}$, let us consider the following RDS of r equations on Γ:

$$\begin{cases} \dot{u}_1 - d_1\Delta_\Gamma u_1 = f_1(u_1,\dots,u_r), \\ \qquad\vdots \qquad\qquad\qquad\qquad (\mathbf{x},t) \in \Gamma\times(0,T], \\ \dot{u}_r - d_r\Delta_\Gamma u_r = f_r(u_1,\dots,u_r), \end{cases} \tag{3.1}$$

where $f_1,\dots,f_r$ are $\mathcal{C}^2(S;\mathbb{R})$ reaction kinetics, with $S \subset \mathbb{R}^r$ being a compact set, and $\mathcal{C}^2(\Gamma)$ initial conditions are given. We further assume that the solutions are bounded in S. Under these assumptions, (3.1) admits a unique global solution (Taylor, 1997, Chapter 15.1). As remarked in Section 1, the following arguments still hold for systems on surfaces with boundary and homogeneous Neumann boundary conditions, i.e., zero *conormal derivative* on $\partial\Gamma$ (see Dziuk & Elliott, 2013a). Therefore, as a special case, planar bounded domains in $\mathbb{R}^2$ with zero-flux boundary conditions could be included in our study. We will confine the present analysis to the case of compact surfaces without boundary to simplify the presentation. In vector form, system (3.1) is given by

$$\begin{cases} \dot{\mathbf{u}} - D\Delta_\Gamma\mathbf{u} = \mathbf{f}(\mathbf{u}), & (\mathbf{x},t) \in \Gamma\times(0,T], \\ \mathbf{u}(\mathbf{x},0) = \mathbf{u}_0(\mathbf{x}), & \mathbf{x} \in \Gamma, \end{cases} \tag{3.2}$$

where $D := \operatorname{diag}(d_1, \dots, d_r)$, $\mathbf{u} := (u_1, \dots, u_r)^{\mathrm{T}}$, $\Delta_\Gamma \mathbf{u} := (\Delta_\Gamma u_1, \dots, \Delta_\Gamma u_r)^{\mathrm{T}}$ and $\mathbf{f}(\mathbf{u}) := (f_1(\mathbf{u}), \dots, f_r(\mathbf{u}))^{\mathrm{T}}$. The weak formulation of (3.1), which requires lower regularity assumptions to be well posed, is given by: find $u_1, \dots, u_r \in L^2([0,T]; H^1(\Gamma)) \cap L^\infty([0,T] \times \Gamma)$ with $\dot{u}_1, \dots, \dot{u}_r \in L^2([0,T]; H^{-1}(\Gamma))$ such that

$$\begin{cases} \displaystyle\int_\Gamma \dot{u}_1 \varphi_1 + d_1 \int_\Gamma \nabla_\Gamma u_1 \cdot \nabla_\Gamma \varphi_1 = \int_\Gamma f_1(\mathbf{u}) \varphi_1 \qquad \forall\, \varphi_1 \in H^1(\Gamma), \\ \qquad\qquad \vdots \\ \displaystyle\int_\Gamma \dot{u}_r \varphi_r + d_r \int_\Gamma \nabla_\Gamma u_r \cdot \nabla_\Gamma \varphi_r = \int_\Gamma f_r(\mathbf{u}) \varphi_r \qquad \forall\, \varphi_r \in H^1(\Gamma), \end{cases} \tag{3.3}$$

where $f_1, \dots, f_r : S \to \mathbb{R}$, with $S \subset \mathbb{R}^r$ being a compact set, are Lipschitz kinetics and the initial conditions are $H^1(\Gamma)$ and bounded in S. We further assume that the solutions to (3.3) are bounded in S. These assumptions are quite standard in the literature on surface PDEs (see, for instance, Dziuk & Elliott, 2013a and references therein). We will require higher regularity assumptions for the convergence results in Theorems 4.8 and 4.9, only. To write the corresponding vector formulation, we extend all the spatial norms considered throughout the article to vector-valued functions $\mathbf{w} : \Gamma \to \mathbb{R}^r$ or $\mathbf{W} : \Gamma_h \to \mathbb{R}^r$ as follows. Given a function space S, we consider the tensor product norm on S^r defined by

$$\|\mathbf{w}\|_{S^r} := \sqrt{\sum_{i=1}^{r} \|w_i\|_S^2} \qquad \forall \mathbf{w} \in S^r. \tag{3.4}$$

For $p \in [1, +\infty]$, the $L^p([0,T]; S^r)$ norms of space- and time-dependent functions $\mathbf{u} : \Gamma \times [0,T] \to \mathbb{R}^r$ are defined accordingly. Without any loss of generality, we can write $\|\cdot\|_S$ and $L^p([0,T]; S)$ instead of $\|\cdot\|_{S^r}$ and $L^p([0,T]; S^r)$. Following Barreira (2009), we introduce the following vector notation:

$$A : B := \sum_{i=1}^{n} \sum_{j=1}^{m} a_{ij} b_{ij} \qquad \forall\, A, B \in \mathbb{R}^{n,m}, \quad \forall\, n, m \in \mathbb{N}.$$

We can now write the sum of equations (3.3) as

$$\int_\Gamma \dot{\mathbf{u}} : \boldsymbol{\varphi} - \int_\Gamma D \nabla_\Gamma \mathbf{u} : \nabla_\Gamma \boldsymbol{\varphi} = \int_\Gamma \mathbf{f}(\mathbf{u}) : \boldsymbol{\varphi} \qquad \forall \boldsymbol{\varphi} \in H^1(\Gamma)^r, \tag{3.5}$$

where $\nabla_\Gamma \mathbf{u}$ is the $r \times 3$ matrix defined by $\nabla_\Gamma \mathbf{u} := (\nabla_\Gamma u_1, \dots, \nabla_\Gamma u_r)^{\mathrm{T}}$.

3.2 *Space discretization*

Analogous to the spatially discretized semilinear parabolic equation (2.6), we define the following space discretization for the RDS (3.3): find $U_1, \dots, U_r \in L^2([0,T]; S_h)$ with $\dot{U}_1, \dots, \dot{U}_r \in L^2([0,T]; S_h)$ such

that

$$\begin{cases} \displaystyle\int_\Gamma I_h(\dot{U}_1\phi_1) + d_1\int_\Gamma \nabla_\Gamma u_1\cdot\nabla_\Gamma\varphi_1 = \int_\Gamma I_h(f_1(\mathbf{U})\phi_1) \qquad \forall\phi_1\in S_h, \\ \qquad\qquad\vdots \\ \displaystyle\int_\Gamma I_h(\dot{U}_r\phi_r) + d_r\int_\Gamma \nabla_\Gamma u_r\cdot\nabla_\Gamma\varphi_r = \int_\Gamma I_h(f_r(\mathbf{U})\phi_r) \qquad \forall\phi_r\in S_h, \end{cases} \tag{3.6}$$

where the initial condition $\mathbf{U}_0(\mathbf{x})$ is the piecewise linear interpolant $I_h(\mathbf{u}_0^{-\ell})(\mathbf{x})$ of the unlifted exact initial condition $\mathbf{u}_0(\mathbf{x})$. By expressing each component u_i according to (2.7), we have the matrix form

$$\begin{cases} \bar{M}\dot{\boldsymbol{\xi}}_1 + d_1A\boldsymbol{\xi}_1 = \bar{M}f_1(\boldsymbol{\xi}_1,\ldots,\boldsymbol{\xi}_r), \\ \qquad\qquad\vdots \\ \bar{M}\dot{\boldsymbol{\xi}}_r + d_rA\boldsymbol{\xi}_r = \bar{M}f_r(\boldsymbol{\xi}_1,\ldots,\boldsymbol{\xi}_r), \end{cases} \tag{3.7}$$

where $\bar{M}$ and A are the lumped mass and stiffness matrices defined in (2.8) and (2.9), respectively.

3.3 *Time discretization*

By applying the IMEX Euler method to (3.6), we obtain the following fully discrete method for (3.3): for all $n = 0,\ldots,N_T$ find $U_1^n,\ldots U_r^n \in S_h$ such that

$$\begin{cases} \displaystyle\int_\Gamma I_h\left(\frac{U_1^{n+1}-U_1^n}{\tau}\phi_1^n\right) + d_1\int_\Gamma \nabla_\Gamma U_1^{n+1}\cdot\nabla_\Gamma\phi_1^n = \int_\Gamma I_h(f_1(\mathbf{U}^n)\phi_1^n), \\ \qquad\qquad\vdots \\ \displaystyle\int_\Gamma I_h\left(\frac{U_r^{n+1}-U_r^n}{\tau}\phi_r^n\right) + d_r\int_\Gamma \nabla_\Gamma U_r^{n+1}\cdot\nabla_\Gamma\phi_r^n = \int_\Gamma I_h(f_r(\mathbf{U}^n)\phi_r^n), \end{cases} \tag{3.8}$$

for all $\phi_1^n,\ldots,\phi_r^n \in S_h$. We can write the sum of equations (3.8) as

$$\int_\Gamma I_h\left(\frac{\mathbf{U}^{n+1}-\mathbf{U}^n}{\tau}:\boldsymbol{\phi}^n\right) + \int_\Gamma D\nabla_\Gamma\mathbf{U}^{n+1}:\nabla_\Gamma\boldsymbol{\phi}^n = \int_\Gamma I_h(\mathbf{f}(\mathbf{U}^n):\boldsymbol{\phi}^n) \tag{3.9}$$

for all $n = 0,\ldots,N_T$ and $\boldsymbol{\phi}^n \in (S_h)^r$. System (3.8) can be written in matrix form as

$$\begin{cases} \boldsymbol{\xi}_1^{n+1} = (\bar{M}+d_1\tau A)^{-1}\bar{M}(\boldsymbol{\xi}_1^n + \tau f_1(\boldsymbol{\xi}_1^n,\ldots,\boldsymbol{\xi}_r^n)), \\ \qquad\qquad\vdots \\ \boldsymbol{\xi}_r^{n+1} = (\bar{M}+d_r\tau A)^{-1}\bar{M}(\boldsymbol{\xi}_r^n + \tau f_r(\boldsymbol{\xi}_1^n,\ldots,\boldsymbol{\xi}_r^n)), \end{cases} \tag{3.10}$$

which can be obtained equivalently by applying the IMEX Euler method directly to the ODE system (3.7).

3.4 *Preservation of the invariant rectangles*

In this section, we investigate an interesting property of the lumped finite element discretization of RDSs, which does not hold in the absence of lumping: the preservation of invariant hyperrectangles. A numerical counterexample will be given in Section 5. This preservation property is crucial when the continuous system is known to have an invariant rectangle for two reasons: (i) the solution might be physically meaningless outside a certain range of feasible values, containing the rectangle and (ii) it is a tool to prove stability estimates and error bounds for the semidiscrete and fully discrete solutions. We recall the following definition (see, for instance, Smoller, 1994; Taylor, 1997).

DEFINITION 3.1 For the system (3.1), a region Σ in the phase space $\mathbb{R}^r$ is said to be a positively invariant region if, whenever the initial condition $\mathbf{u}_0$ is in Σ, $\mathbf{u}$ stays in Σ as long as it exists and is unique.

The following theorem has been proved in Smoller (1994) when Γ is a monodimensional domain in $\mathbb{R}$, in Chueh *et al.* (1977) when Γ is a k-dimensional domain in $\mathbb{R}^k$, $k \in \mathbb{N}$ (zero-flux boundary conditions are enforced if the domain is not the whole space) and in Taylor (1997) when Γ is a Riemannian manifold without boundary. This latter result provides a sufficient condition for Σ to be a positively invariant region in the phase space.

THEOREM 3.2 (Invariant rectangles for the continuous system (3.1); Taylor, 1997, Chapter 15, Proposition 4.3) Let $\Sigma = \prod_{k=1}^{r} [m_k, M_k]$ be a hyperrectangle in the phase space of (3.1), and let $\mathbf{n}$ be the unit outward vector defined piecewise on $\partial\Sigma$. If

$$\mathbf{f}(\mathbf{u}) \cdot \mathbf{n}(\mathbf{u}) < 0 \qquad \forall\, \mathbf{u} \in \partial\Sigma \tag{3.11}$$

then Σ is an invariant region for (3.1). □

We remark that some systems are known to possess an invariant region which do not meet the strict inequality (3.11). For instance, for many mass-action laws, the positive orthant is invariant (see Chellaboina *et al.*, 2009) even though the flow of $\mathbf{f}$ is tangent to this region, instead of strictly inward.

In the following theorems we prove that, under the same assumptions, Σ is an invariant region for the semidiscrete problem (3.6) and for the fully discrete solution (3.10) conditionally on τ, as well. Furthermore, we will relax the strict inequality (3.11) as stated in the following Corollary 3.4 and Theorem 3.5.

THEOREM 3.3 (Invariant rectangles for (3.6)) Let

$$\Sigma = \prod_{k=1}^{r} [m_k, M_k] \tag{3.12}$$

be a hyperrectangle in the phase space of (3.6), let $\mathbf{n}$ be the outward unit normal defined piecewise on $\partial\Sigma$ and assume the Delaunay condition (2.11). If

$$\mathbf{f}(\mathbf{u}) \cdot \mathbf{n}(\mathbf{u}) < 0 \qquad \forall\, \mathbf{u} \in \partial\Sigma, \tag{3.13}$$

then Σ is an invariant region for the semidiscrete problem (3.6).

Proof. We rewrite the semidiscrete problem (3.7) as

$$\begin{pmatrix} \dot{\boldsymbol{\xi}}_1 \\ \vdots \\ \dot{\boldsymbol{\xi}}_r \end{pmatrix} = - \begin{pmatrix} d_1 \bar{M}^{-1} A & & 0 \\ & \ddots & \\ 0 & & d_r \bar{M}^{-1} A \end{pmatrix} \begin{pmatrix} \boldsymbol{\xi}_1 \\ \vdots \\ \boldsymbol{\xi}_r \end{pmatrix} + \begin{pmatrix} f_1(\boldsymbol{\xi}_1, \ldots, \boldsymbol{\xi}_r) \\ \vdots \\ f_r(\boldsymbol{\xi}_1, \ldots, \boldsymbol{\xi}_r) \end{pmatrix}. \tag{3.14}$$

All we need to prove is that the rN-dimensional rectangle $\bar{\Sigma} = \prod_{k=1}^{r} [m_k, M_k]^N$ is an invariant region for the ODE system (3.14). To this end, suppose that, at some $\bar{t} > 0$, the semidiscrete solution $(\boldsymbol{\xi}_1(\bar{t}), \ldots, \boldsymbol{\xi}_r(\bar{t}))^{\mathrm{T}}$ is on $\partial\bar{\Sigma}$. This means that there exist $i = 1, \ldots, N$ and $k = 1, \ldots, r$ such that $\xi_{k,i}(\bar{t}) \in \{m_k, M_k\}$. Suppose $\xi_{k,i}(\bar{t}) = M_k$; in the case $\xi_{k,i}(\bar{t}) = m_k$ the proof is analogous. Then

$$\xi_{k,j}(\bar{t}) \leq \xi_{k,i}(\bar{t}), \quad j \neq i. \tag{3.15}$$

All we have to prove is that $\dot{\xi}_{k,i}(\bar{t}) < 0$. To see this, consider that

1. $f_k(\xi_{1,i}(\bar{t}), \ldots, \xi_{r,i}(\bar{t})) = f_k(\xi_{1,i}(\bar{t}), \ldots, M_k, \ldots, \xi_{r,i}(\bar{t})) < 0$ from (3.13);
2. the ith component of the vector $-d_k \bar{M}^{-1} A \boldsymbol{\xi}_k(\bar{t})$ is nonpositive. The proof of this condition is exactly identical to that of Theorem 2.1 and for the sake of brevity we omit the details.

This completes the proof. □

COROLLARY 3.4 (Invariant rectangles for (3.6)) Let $\Sigma_p = \prod_{k=1}^{r} [m_k^p, M_k^p]$, $p \in \mathbb{N}$ be a sequence of hyperrectangles in the phase space of (3.6) such that $\Sigma^{p+1} \subset \Sigma^p$ for all $p \in \mathbb{N}$ and $\Sigma^p \to \Sigma$ for $p \to +\infty$, with Σ as defined in (3.12). For all $p \in \mathbb{N}$, let $\mathbf{n}_p$ be the outward unit normal defined piecewise on $\partial\Sigma^p$ and suppose that

$$\mathbf{f}(\mathbf{u}) \cdot \mathbf{n}_p(\mathbf{u}) < 0 \qquad \forall\, \mathbf{u} \in \partial\Sigma^p. \tag{3.16}$$

Then Σ is an invariant region for the semidiscrete problem (3.6).

Proof. From Theorem 3.3 we have that, for all $p \in \mathbb{N}$, Σ^p is invariant for (3.6). Now, since the intersection of invariant regions is still invariant, we have that $\Sigma = \bigcap_{p \in \mathbb{N}} \Sigma^p$ is invariant for (3.6), which completes the proof. □

We remark that, from Corollary 3.4, a region Σ can be invariant for the semidiscrete system (3.6) even when the flux of the kinetics through $\partial\Sigma$ vanishes, i.e., $\mathbf{f}(\mathbf{u}) \cdot \mathbf{n} = 0$ for all $\mathbf{u} \in \partial\Sigma$. The following theorem is a fully discrete counterpart of Theorem 3.3. Observe that the strictly inward flux condition (3.13) is replaced by a weaker requirement. This makes the fully discrete scheme (3.10) somehow more stable than the spatially discrete one (3.6). The reason for this is that, given a trajectory $u(\mathbf{x}, t)$ whose time derivative vanishes at $(\bar{\mathbf{x}}, \bar{t})$, the function $t \mapsto u(\bar{\mathbf{x}}, t)$ might still be strictly monotonic, this means that a trajectory may escape a region Σ even though the flux of the kinetics is tangent to $\partial\Sigma$.

THEOREM 3.5 (Invariant rectangles for (3.10)) Let $\Sigma = \prod_{k=1}^{r}[m_k, M_k]$ be a region in the phase space such that

$$\mathbf{f}(\mathbf{u}) \cdot \mathbf{n}(\mathbf{u}) \leq 0 \qquad \forall\, \mathbf{u} \in \partial\Sigma. \tag{3.17}$$

For all $k = 1, \ldots, r$, let L_k be the Lipschitz constant of f_k on Σ. Then, under the Delaunay condition (2.11), Σ is an invariant region for the scheme (3.10) if the timestep τ fulfils

$$\tau \leq \frac{1}{\max\limits_{k=1,\ldots,r}(L_k)}. \tag{3.18}$$

Proof. From the matrix properties (2.14) and (2.15) it follows that, for every $\tau > 0$,

$$(\bar{M} + d_k \tau A)^{-1}\bar{M} \geq \mathbf{0} \qquad \forall\, k = 1, \ldots, r,$$
$$(\bar{M} + d_k \tau A)^{-1}\bar{M}\mathbf{1} = \mathbf{1} \qquad \forall\, k = 1, \ldots, r.$$

For the fully discrete scheme (3.10) to fulfil the theorem, it remains to ensure that

$$m_k \leq \xi_{k,i}^n + \tau f_k(\xi_{1,i}^n, \ldots, \xi_{r,i}^n) \leq M_k \quad \forall\, k = 1, \ldots, r,\ \forall\, i = 1, \ldots, N,\ \forall\, n = 0, \ldots, N_T. \tag{3.19}$$

Condition (3.19) is equivalent to

$$\tau \leq \frac{M_k - \xi_{k,i}^n}{f_k\left(\xi_{1,i}^n, \ldots, \xi_{r,i}^n\right)} \qquad \forall\, i \ \text{ s.t.}\, f_k\left(\xi_{1,i}^n, \ldots, \xi_{r,i}^n\right) > 0, \tag{3.20}$$

$$\tau \leq \frac{m_k - \xi_{k,i}^n}{f_k\left(\xi_{i,1}^n, \ldots, \xi_{r,i}^n\right)} \qquad \forall\, i \ \text{ s.t.}\, f_k\left(\xi_{1,i}^n, \ldots, \xi_{r,i}^n\right) < 0, \tag{3.21}$$

for all $k = 1, \ldots, r$ and $n = 0, \ldots, N_T$. If $f_k\left(\xi_{1,i}^n, \ldots, \xi_{k,i}^n\right) > 0$ then

$$f_k\left(\xi_{1,i}^n, \ldots, \xi_{r,i}^n\right) \leq f_k(M_k) + L_k\left(M_k - \xi_{k,i}^n\right) \underset{(3.17)}{\leq} L_k\left(M_k - \xi_{k,i}^n\right). \tag{3.22}$$

If, instead, $f_k(\xi_{1,i}^n, \ldots, \xi_{k,i}^n) < 0$ then

$$f_k\left(\xi_{1,i}^n, \ldots, \xi_{r,i}^n\right) \geq f_k(m_k) - L_k\left(\xi_{k,i}^n - m_k\right) \underset{(3.17)}{\geq} -L_k\left(\xi_{k,i}^n - m_k\right). \tag{3.23}$$

Using (3.22) and (3.23), then (3.20) and (3.21) hold if $\tau \leq \frac{1}{L_k}$ for all $k = 1, \ldots, r$, which is true by assumption. This completes the proof. □

4. Stability and error analysis

In this section, we will prove stability estimates and optimal $L^\infty([0,T], L^2(\Gamma))$ error bounds for the semidiscrete (3.6) and the fully discrete (3.10) solutions of the RDS (3.1) of $r \in \mathbb{N}$ equations. This analysis includes the semilinear parabolic equation (2.2), that is a special case of system (3.1) for $r = 1$

and $f(u) = -\beta u^\alpha$ for which the maximum principle $0 \le u \le \max u_0$ corresponds to the existence of the invariant regions $[0, M]$ for all $M > 0$. Next, we introduce some preliminaries and some basic notation.

The lumped L^2 product (see, for instance, Thomée, 1984; Nie & Thomée, 1985; Nochetto & Verdi, 1996; Garvie & Trenchea, 2007) defined by

$$(U, V)_h := \int_{\Gamma_h} I_h(UV) \qquad \forall\, U, V \in L^2(\Gamma_h), \tag{4.1}$$

where I_h is given in (2.5), induces the following norm on S_h,

$$\|U\|_h = \sqrt{(U, U)_h} \qquad \forall\, U \in S_h,$$

which is equivalent to $\|\cdot\|_{L^2(\Gamma_h)}$, uniformly with respect to h (see Raviart, 1973 for the proof):

$$\|U\|_{L^2(\Gamma_h)} \le \|U\|_h \le C\|U\|_{L^2(\Gamma_h)} \qquad \forall\, U \in S_h,\ \forall\, h > 0. \tag{4.2}$$

Let us define the 'broken' Sobolev space as

$$H_h^2(\Gamma_h) := H^1(\Gamma_h) \cap \prod_{K \in \mathcal{K}_h} H^2(K),$$

endowed with the norm and the seminorm defined by

$$\|U\|^2_{H_h^2(\Gamma_h)} := \sum_{K \in \mathcal{K}_h} \|U\|^2_{H^2(K)} \quad \text{and} \qquad |U|^2_{H_h^2(\Gamma_h)} := \sum_{K \in \mathcal{K}_h} |U|^2_{H^2(K)}, \qquad \forall\, U \in H_h^2(\Gamma_h), \tag{4.3}$$

respectively. For the error in the lumped quadrature rule (4.1), if $U \in H_h^2(\Gamma_h)$ and $V \in S_h$ then the following estimate holds (see Nie & Thomée, 1985):

$$|\varepsilon_h(U, V)| := \left| \int_{\Gamma_h} (UV - I_h(UV)) \right| \le ch^2 \|U\|_{H_h^2(\Gamma_h)} \|V\|_{H^1(\Gamma_h)}. \tag{4.4}$$

Inequalities (4.2) and (4.4) have been proved on planar triangulations in Raviart (1973) and Nie & Thomée (1985), respectively. However, since the respective proofs are done piecewise on each triangle, they can be trivially extended to triangulated surfaces with an affine map argument.

The following equivalences between the norms of a function U defined on Γ_h and its lifted counterpart U^ℓ can be found in Dziuk & Elliott (2013a).

LEMMA 4.1 Let $K \in \mathcal{K}_h$, $\tilde{K} := \mathbf{a}(K) \subset \Gamma$, where the map $\mathbf{a}(\mathbf{x})$ is given in (2.1), and $U : K \to \mathbb{R}$. If the norms exist then the following inequalities hold:

$$c\|U\|_{L^2(K)} \le \left\|U^\ell\right\|_{L^2(\tilde{K})} \le C\|U\|_{L^2(K)}, \tag{4.5}$$

$$c\|\nabla_T U\|_{L^2(K)} \le \left\|\nabla_{\tilde{K}} U^\ell\right\|_{L^2(\tilde{K})} \le C\|\nabla_K U\|_{L^2(K)}, \tag{4.6}$$

$$\left\|\nabla_K^2 U\right\|_{L^2(K)} \le c\left(\left\|\nabla_{\tilde{K}}^2 U^\ell\right\|_{L^2(\tilde{K})} + h\left\|\nabla_{\tilde{K}} U^\ell\right\|_{L^2(\tilde{K})}\right), \tag{4.7}$$

where ∇^2_K and $\nabla^2_{\tilde{K}}$ are the tangential Hessians on K and $\tilde{K}$, respectively. □

From the previous lemma, we derive the following estimate for the broken H^2 norm of U.

LEMMA 4.2 If $u \in H^2(\Gamma)$ then $u^{-\ell} \in H^2_h(\Gamma_h)$ and

$$\left\|u^{-\ell}\right\|_{H^2_h(\Gamma_h)} \leq C(1+h)\|u\|_{H^2(\Gamma)}. \tag{4.8}$$

Proof. Let $K \in \mathcal{K}_h$. From (4.5) to (4.7), we have

$$\begin{aligned}\left\|u^{-\ell}\right\|^2_{H^2(K)} &= \left\|u^{-\ell}\right\|^2_{L^2(K)} + \left\|\nabla_K u^{-\ell}\right\|^2_{L^2(K)} + \left\|\nabla^2_K u^{-\ell}\right\|^2_{L^2(K)} \leq \frac{1}{c^2}\|u\|^2_{L^2(\tilde{K})} + \frac{1}{c^2}\|\nabla_{\tilde{K}} u\|^2_{L^2(\tilde{K})} \\ &\quad + c^2\left\|\nabla^2_{\tilde{K}} u\right\|^2_{L^2(\tilde{K})} + c^2h^2\|\nabla_{\tilde{K}} u\|^2_{L^2(\tilde{K})} \leq C\left(1+h^2\right)\|u\|^2_{H^2(\tilde{K})}.\end{aligned} \tag{4.9}$$

Hence from (4.9), we have

$$\left\|u^{-\ell}\right\|^2_{H^2_h(\Gamma_h)} = \sum_{K\in\mathcal{K}_h}\left\|u^{-\ell}\right\|^2_{H^2(K)} \underset{(4.9)}{\leq} C(1+h^2)\sum_{K\in\mathcal{K}_h}\|u\|^2_{H^2(\tilde{K})} \leq C\left(1+h^2\right)\|u\|^2_{H^2_h(\Gamma)}. \tag{4.10}$$

We remark that, in the last inequality of (4.10), the exact equality might not hold, since $u^{-\ell}$ being only $H^2_h(\Gamma_h)$, its gradient $\nabla_{\Gamma_h} u^{-\ell}$ might have finite jumps across the edges of the triangulation $\mathcal{K}_h$. This completes the proof. □

When lifting integrals, a geometric error must be taken into account. The following equalities hold (see Dziuk & Elliott, 2013a, p. 317):

$$\int_{\Gamma_h} UV = \int_{\Gamma} \frac{U^\ell V^\ell}{\delta^\ell_h} \qquad \forall\, U, V \in L^2(\Gamma_h), \tag{4.11}$$

$$\int_{\Gamma_h} \nabla_{\Gamma_h} U \cdot \nabla_{\Gamma_h} V = \int_{\Gamma} \nabla_\Gamma U^\ell R^T_h \cdot \nabla_\Gamma V^\ell \qquad \forall\, U, V \in H^1(\Gamma_h), \tag{4.12}$$

where $\delta^\ell_h : \Gamma \to \mathbb{R}$ and $R^T_h : \Gamma \to \mathbb{R}^{3,3}$ are functions such that (see Dziuk & Elliott, 2013a, p. 310)

$$\left\|1 - \frac{1}{\delta^\ell_h}\right\|_{L^\infty(\Gamma)} \leq Ch^2, \tag{4.13}$$

$$\|I - R_h\|_{L^\infty(\Gamma)} \leq Ch^2. \tag{4.14}$$

For the following proofs, we need to define the seminorm $|\cdot|_D$ on $(H^1(\Gamma))^r$ and $(H^1(\Gamma_h))^r$ by

$$|\mathbf{u}|^2_D := \int_\Gamma D\nabla_\Gamma \mathbf{u} : \nabla_\Gamma \mathbf{u} \qquad \forall\, \mathbf{u} \in H^1(\Gamma)^r, \tag{4.15}$$

$$|\mathbf{U}|^2_D := \int_{\Gamma_h} D\nabla_{\Gamma_h} \mathbf{U} : \nabla_{\Gamma_h} \mathbf{U} \qquad \forall\, \mathbf{U} \in H^1(\Gamma_h)^r, \tag{4.16}$$

respectively. Since the diffusion matrix D is diagonal with positive entries, it holds that

$$\min_{k=1,\dots,r}(d_k)|\mathbf{u}|^2_{H^1(\Gamma)} \le |\mathbf{u}|^2_D \le \max_{k=1,\dots,r}(d_k)|\mathbf{u}|^2_{H^1(\Gamma)} \qquad \forall\, \mathbf{u} \in (H^1(\Gamma))^r, \tag{4.17}$$

$$\min_{k=1,\dots,r}(d_k)|\mathbf{U}|^2_{H^1(\Gamma_h)} \le |\mathbf{U}|^2_D \le \max_{k=1,\dots,r}(d_k)|\mathbf{U}|^2_{H^1(\Gamma_h)} \quad \forall\, \mathbf{U} \in (H^1(\Gamma_h))^r, \tag{4.18}$$

i.e., the norms (4.15) and (4.16) are equivalent to $|\cdot|_{H^1(\Gamma)}$ and $|\cdot|_{H^1(\Gamma_h)}$, respectively.

The following stability estimates are carried out with the usual energy arguments. However, thanks to the existence of an invariant region, the estimates will not depend exponentially on time, since the proofs will not rely on Grönwall's lemma. Moreover, we require that the reaction kinetics $\mathbf{f}$ in (3.2) are Lipschitz only in the invariant region, instead of being globally Lipschitz.

LEMMA 4.3 (Stability estimates for the weak system (3.3)) If $\mathbf{u}$ is the solution of (3.3), $\Sigma = \prod_{k=1}^r [m_k, M_k]$ is an invariant region for (3.3), and $\mathbf{u}_0 \in \Sigma$ then

$$\sup_{t\in[0,T]} ||\mathbf{u}||^2_{L^2(\Gamma)} + \int_0^T \|\nabla_\Gamma \mathbf{u}\|^2_{L^2(\Gamma)} \le C\left(T + \|\mathbf{u}_0\|^2_{L^2(\Gamma)}\right), \tag{4.19}$$

$$\int_0^T \|\dot{\mathbf{u}}\|^2_{L^2(\Gamma)} + \sup_{t\in[0,T]} \|\nabla_\Gamma \mathbf{u}\|^2_{L^2(\Gamma)} \le C\left(T + \|\nabla_\Gamma \mathbf{u}_0\|^2_{L^2(\Gamma)}\right), \tag{4.20}$$

for all $T > 0$, where C is a constant independent of T and $\mathbf{u}_0$.

Proof. By setting $\boldsymbol{\varphi} = \mathbf{u}$ in (3.5), we have

$$\frac{1}{2}\frac{\mathrm{d}}{\mathrm{d}t}\int_\Gamma |\mathbf{u}|^2 + |\mathbf{u}|^2_D = \int_\Gamma \mathbf{f}(\mathbf{u}) : \mathbf{u}. \tag{4.21}$$

Combining (4.17) and (4.21), we have

$$\frac{\mathrm{d}}{\mathrm{d}t}\|\mathbf{u}\|^2_{L^2(\Gamma)} + |\mathbf{u}|^2_{H^1(\Gamma)} \le C\int_\Gamma |\mathbf{f}(\mathbf{u}) : \mathbf{u}|.$$

Since $\mathbf{u} \in \Sigma$ at all times and $\mathbf{f}$ is bounded on Σ, we obtain

$$\frac{\mathrm{d}}{\mathrm{d}t}\|\mathbf{u}\|^2_{L^2(\Gamma)} + |\mathbf{u}|^2_{H^1(\Gamma)} \le C. \tag{4.22}$$

By integrating both sides of (4.22) over $[0, T]$, estimate (4.19) follows.

To prove the second estimate, we set $\boldsymbol{\varphi} = \dot{\mathbf{u}}$ in (3.5) and obtain

$$\int_\Gamma |\dot{\mathbf{u}}|^2 + \frac{1}{2}\frac{\mathrm{d}}{\mathrm{d}t}\int_\Gamma D\nabla_\Gamma \mathbf{u} : \nabla_\Gamma \mathbf{u} \le \int_\Gamma |\mathbf{f}(\mathbf{u})||\dot{\mathbf{u}}|, \tag{4.23}$$

but, since $\mathbf{f}$ is bounded in Σ, we have

$$\int_\Gamma |\mathbf{f}(\mathbf{u})||\dot{\mathbf{u}}| \le \frac{1}{2}\int_\Gamma |\mathbf{f}(\mathbf{u})|^2 + \frac{1}{2}\int_\Gamma |\dot{\mathbf{u}}|^2 \le C + \frac{1}{2}\int_\Gamma |\dot{\mathbf{u}}|. \tag{4.24}$$

Combining (4.23) and (4.24) we have $\|\dot{\mathbf{u}}\|^2_{L^2(\Gamma)} + \frac{\mathrm{d}}{\mathrm{d}t}|\mathbf{u}|^2_D \leq C$, from which, by integrating on $[0,T]$, we obtain

$$\int_0^T \|\dot{\mathbf{u}}\|^2_{L^2(\Gamma)} + |\mathbf{u}|^2_D \leq CT + |\mathbf{u}_0|^2_D. \tag{4.25}$$

Similarly, combining (4.25) with (4.17), we have

$$\int_0^T \|\dot{\mathbf{u}}\|^2_{L^2(\Gamma)} + |\mathbf{u}|^2_{H^1(\Gamma)} \leq C\left(T + |\mathbf{u}_0|^2_{H^1(\Gamma)}\right),$$

from which we obtain estimate (4.20). □

The following lemmas show analogous estimates for the semidiscrete and fully discrete problems.

LEMMA 4.4 (Stability estimates for the semidiscrete system (3.6)) If $\mathbf{U}$ is the solution of (3.6), $\Sigma = \prod_{k=1}^r [m_k, M_k]$ is an invariant region for (3.6), and $\mathbf{U}_0 \in \Sigma$ then

$$\sup_{t\in[0,T]} ||\mathbf{U}||^2_{L^2(\Gamma_h)} + \int_0^T \|\nabla_\Gamma \mathbf{U}\|^2_{L^2(\Gamma_h)} \leq C\left(T + \|\mathbf{U}_0\|^2_{L^2(\Gamma_h)}\right), \tag{4.26}$$

$$\int_0^T \|\dot{\mathbf{U}}\|^2_{L^2(\Gamma_h)} + \sup_{t\in[0,T]} \|\nabla_\Gamma \mathbf{U}\|^2_{L^2(\Gamma_h)} \leq C\left(T + \|\nabla_\Gamma \mathbf{U}_0\|^2_{L^2(\Gamma_h)}\right), \tag{4.27}$$

for all $T > 0$, where C is a constant independent of T and $\mathbf{U}_0$.

Proof. We proceed exactly as in the previous lemma to obtain analogous estimates in the norm $\|\cdot\|_h$ and then we use the equivalence (4.2) between the norms $\|\cdot\|_h$ and $\|\cdot\|_{L^2(\Gamma_h)}$ on S_h, uniformly in h. □

LEMMA 4.5 (Stability estimates for the fully discrete system (3.8)) Let $\tau > 0$. If $\mathbf{U}^i$, $i = 0, \ldots, N_T$ is the solution of (3.8), $\Sigma = \prod_{k=1}^r [m_k, M_k]$ is an invariant region for (3.8) and $\mathbf{U}_0 \in \Sigma$ then

$$\left\|\mathbf{U}^{n+1}\right\|^2_{L^2(\Gamma_h)} + \tau \sum_{i=0}^n \left\|\nabla_{\Gamma_h} \mathbf{U}^{i+1}\right\|^2_{L^2(\Gamma_h)} \leq C(\|\mathbf{U}^0\|_{L^2(\Gamma_h)} + T), \tag{4.28}$$

$$\frac{1}{\tau}\sum_{i=0}^n \left\|\mathbf{U}^{i+1} - \mathbf{U}^i\right\|^2_{L^2(\Gamma_h)} + \left\|\nabla_{\Gamma_h} \mathbf{U}^{n+1}\right\|^2_{L^2(\Gamma_h)} \leq C\left(\left\|\nabla_{\Gamma_h} \mathbf{U}^0\right\|^2_{L^2(\Gamma_h)} + T\right), \tag{4.29}$$

for all $n = 0, \ldots, N_T$ and $T > 0$, where C is a constant independent of T and $\mathbf{U}_0$.

Proof. By testing (3.9) with $\boldsymbol{\phi}^i = \mathbf{U}^{i+1}$, we have

$$\frac{1}{\tau}\left(\left\|\mathbf{U}^{i+1}\right\|^2_h - \int_{\Gamma_h} I_h\left(\mathbf{U}^i : \mathbf{U}^{i+1}\right)\right) + \left|\mathbf{U}^{i+1}\right|^2_D = \int_{\Gamma_h} I_h\left(\mathbf{f}(\mathbf{U}^i) : \mathbf{U}^{i+1}\right).$$

After multiplying by τ, the Cauchy–Schwarz inequality yields

$$\left\|\mathbf{U}^{i+1}\right\|_h^2 + \tau \left|\mathbf{U}^{i+1}\right|_D^2 \leq \left\|\mathbf{U}^{i+1}\right\|_h \left\|\mathbf{U}^{i}\right\|_h + \tau \left\|\mathbf{f}(\mathbf{U})^i\right\|_h \left\|\mathbf{U}^{i+1}\right\|_h.$$

Since $\mathbf{U}^i$ and $\mathbf{U}^{i+1} \in \Sigma$ and $\mathbf{f}$ is Lipschitz in Σ, the last term on the right-hand side is bounded by some constant $C > 0$:

$$\left\|\mathbf{U}^{i+1}\right\|_h^2 + \tau \left|\mathbf{U}^{i+1}\right|_D^2 \leq \left\|\mathbf{U}^{i+1}\right\|_h \left\|\mathbf{U}^{i}\right\|_h + C\tau.$$

Young's inequality yields

$$\|\mathbf{U}^{i+1}\|_h^2 + \tau |\mathbf{U}^{i+1}|_D^2 \leq \|\mathbf{U}^{i}\|_h^2 + C\tau.$$

We sum for $i = 0, \ldots, n$ to obtain

$$\left\|\mathbf{U}^{n+1}\right\|_h^2 + \tau \sum_{i=0}^{n} \left|\mathbf{U}^{i+1}\right|_D^2 \leq \left\|\mathbf{U}^{0}\right\|_h^2 + Cn\tau.$$

By using (4.2), the equivalence between $|\cdot|_D$ and $|\cdot|_{H^1(\Gamma_h)}$ and $n = 0, \ldots, N_T$, inequality (4.28) follows immediately.

By testing (3.9) with $\boldsymbol{\phi}^i = \mathbf{U}^{i+1} - \mathbf{U}^i$ we have

$$\frac{1}{\tau}\left\|\mathbf{U}^{i+1} - \mathbf{U}^i\right\|_h^2 + \left|\mathbf{U}^{i+1}\right|_D^2 - \int_{\Gamma_h} D\nabla_{\Gamma_h}\mathbf{U}^{i+1} : \nabla_{\Gamma_h}\mathbf{U}^i = \int_{\Gamma_h} I_h(\mathbf{f}(\mathbf{U}^i) : (\mathbf{U}^{i+1} - \mathbf{U}^i)).$$

The Cauchy–Schwarz inequality yields

$$\frac{1}{\tau}\left\|\mathbf{U}^{i+1} - \mathbf{U}^i\right\|_h^2 + \left|\mathbf{U}^{i+1}\right|_D^2 \leq \left|\mathbf{U}^{i+1}\right|_D \left|\mathbf{U}^{i}\right|_D + \left\|\mathbf{f}\left(\mathbf{U}^i\right)\right\|_h \left\|\mathbf{U}^{i+1} - \mathbf{U}^i\right\|_h.$$

Since $\mathbf{f}$ is Lipschitz, and thus bounded, in Σ, say $\max_\Sigma \mathbf{f} = C$, we can bound the last term on the right-hand side as

$$\frac{1}{\tau}\|\mathbf{U}^{i+1} - \mathbf{U}^i\|_h^2 + |\mathbf{U}^{i+1}|_D^2 \leq |\mathbf{U}^{i+1}|_D |\mathbf{U}^i|_D + C\|\mathbf{U}^{i+1} - \mathbf{U}^i\|_h.$$

Young's inequality yields

$$\frac{1}{\tau}\|\mathbf{U}^{i+1} - \mathbf{U}^i\|_h^2 + |\mathbf{U}^{i+1}|_D^2 \leq \frac{1}{2}(|\mathbf{U}^i|_D^2 + |\mathbf{U}^{i+1}|_D^2) + C\tau + \frac{1}{2\tau}\|\mathbf{U}^{i+1} - \mathbf{U}^i\|_h^2.$$

Rearranging terms and multiplying by 2, we have

$$\frac{1}{\tau}\left\|\mathbf{U}^{i+1} - \mathbf{U}^i\right\|_h^2 + \left|\mathbf{U}^{i+1}\right|_D^2 \leq \left|\mathbf{U}^{i}\right|_D^2 + C\tau. \tag{4.30}$$

By summing (4.30) for $i = 0, \ldots, n$ we have

$$\frac{1}{\tau}\sum_{i=0}^{n}\left\|\mathbf{U}^{i+1} - \mathbf{U}^i\right\|_h^2 + \left|\mathbf{U}^{n+1}\right|_D^2 \leq \left|\mathbf{U}^{0}\right|_D^2 + Cn\tau.$$

By using (4.2), the equivalence between $|\cdot|_D$ and $|\cdot|_{H^1(\Gamma_h)}$ and $n = 0, \ldots, N_T$, (4.29) finally follows. □

To prove the convergence of the semidiscrete and fully discrete methods, we will adopt the surface Ritz projection considered in Du *et al.* (2011) and Elliott & Ranner (2015).

DEFINITION 4.6 Given $u : [0,T] \to H^1(\Gamma)$, the Ritz projection of u is the unique function $\bar{U} : [0,T] \to S_h$ such that

$$\int_{\Gamma_h} \nabla_{\Gamma_h} \bar{U} \cdot \nabla_{\Gamma_h} \varphi = \int_{\Gamma} \nabla_{\Gamma} u \cdot \nabla_{\Gamma} \varphi^{\ell} \quad \text{and} \quad \int_{\Gamma_h} \bar{U} = \int_{\Gamma} u \qquad \forall\, \varphi \in S_h. \tag{4.31}$$

We remark that this definition is different from the one considered in Dziuk & Elliott (2013b). The following error estimates for the Ritz projection can be found in Du *et al.* (2011) and Elliott & Ranner (2015).

THEOREM 4.7 (Error estimates for the Ritz projection) Given $u : [0,T] \to H^2(\Gamma)$ such that $\dot{u} : [0,T] \to H^2(\Gamma)$, the error in the Ritz projection satisfies the bounds

$$\left\| u - \bar{U}^{\ell} \right\|_{L^2(\Gamma)} + h \left\| \nabla_{\Gamma} (u - \bar{U}^{\ell}) \right\|_{L^2(\Gamma)} \leq c h^2 \|u\|_{H^2(\Gamma)}, \tag{4.32}$$

$$\left\| \dot{u} - \dot{\bar{U}}^{\ell} \right\|_{L^2(\Gamma)} + h \left\| \nabla_{\Gamma} \left(\dot{u} - \dot{\bar{U}}^{\ell} \right) \right\|_{L^2(\Gamma)} \leq c h^2 \left(\|u\|_{H^2(\Gamma)} + \|\dot{u}\|_{H^2(\Gamma)} \right). \tag{4.33}$$

□

If $\mathbf{u}$ is a vector function, we will denote by $\bar{\mathbf{U}}$ its componentwise Ritz projection and the estimates (4.32)–(4.33) still hold in the tensor product norms (3.4). An $L^{\infty}([0,T], L^2(\Gamma))$ error bound for the semidiscrete solution has been proved in Nie & Thomée (1985) on planar domains. Here, we extend this result to triangulated surfaces.

THEOREM 4.8 (Error estimate for the semidiscrete solution (3.6)) Assume that Σ is an invariant region for (3.3) and (3.6), that $\mathbf{f} \in \mathcal{C}^2(\Sigma)$ and that $\mathbf{u}_0, \mathbf{U}_0 \in \Sigma$. If the solution $\mathbf{u}$ of (3.3) and its time derivative $\dot{\mathbf{u}}$ are $L^{\infty}([0,T]; H^2(\Gamma))$ and $\|\mathbf{u}_0 - \mathbf{U}_0^{\ell}\|_{L^2(\Gamma)} \leq c h^2$ then the following estimate holds:

$$\|\mathbf{u} - \mathbf{U}^{\ell}\|_{L^2(\Gamma)} \leq C(\mathbf{u}, T) h^2, \tag{4.34}$$

where $C(\mathbf{u}, T)$ is a constant depending on $\mathbf{u}$ and T.

Proof. Let us write the error as

$$\mathbf{U}^{\ell} - \mathbf{u} = \left(\mathbf{U}^{\ell} - \bar{\mathbf{U}}^{\ell} \right) + \left(\bar{\mathbf{U}}^{\ell} - \mathbf{u} \right) =: \boldsymbol{\theta}^{\ell} + \boldsymbol{\rho}^{\ell}. \tag{4.35}$$

Since $\mathbf{u}$ and $\dot{\mathbf{u}}$ are $L^{\infty}([0,T], H^2(\Gamma))$, from the error estimates (4.32)–(4.33) for the Ritz projection and (4.5)–(4.6), we have

$$\|\boldsymbol{\rho}\|_{L^2(\Gamma_h)} \leq C \|\boldsymbol{\rho}^{\ell}\|_{L^2(\Gamma)} = C \|\bar{\mathbf{U}}^{\ell} - \mathbf{u}\|_{L^2(\Gamma)} \leq C h^2 \|\mathbf{u}\|_{H^2(\Gamma)}, \tag{4.36}$$

$$\|\dot{\boldsymbol{\rho}}\|_{L^2(\Gamma_h)} + h \|\nabla_{\Gamma_h} \dot{\boldsymbol{\rho}}\|_{L^2(\Gamma_h)} \leq C h^2 \left(\|\mathbf{u}\|_{H^2(\Gamma)} + \|\dot{\mathbf{u}}\|_{H^2(\Gamma)} \right). \tag{4.37}$$

It remains to show the convergence for $\boldsymbol{\theta}^\ell$ in (4.35). For the sake of simplicity, we derive an estimate for $\boldsymbol{\theta}$ in the norm $\|\cdot\|_h$ and then we will use (4.2) and (4.5) to estimate $\|\boldsymbol{\theta}^\ell\|_{L^2(\Gamma)}$. The continuous problem (3.3), the semidiscrete formulation (3.6), the definition of the Ritz projection (4.31) and the relations (4.11) and (4.12) imply that

$$\begin{aligned}\int_{\Gamma_h} I_h(\dot{\boldsymbol{\theta}} : \boldsymbol{\phi}) + \int_{\Gamma_h} D\nabla_{\Gamma_h}\boldsymbol{\theta} : \nabla_{\Gamma_h}\boldsymbol{\phi} &= \int_{\Gamma_h} I_h((\mathbf{f}(\mathbf{U}) - \mathbf{f}(\mathbf{u}^{-\ell})) : \boldsymbol{\phi}) - \varepsilon_h(\mathbf{f}(\mathbf{u}^{-\ell}), \boldsymbol{\phi}) \\ &\quad - \int_\Gamma \left(1 - \frac{1}{\delta_h^\ell}\right)\mathbf{f}(\mathbf{u}) : \boldsymbol{\phi}^\ell - \int_{\Gamma_h} \dot{\boldsymbol{\rho}} : \boldsymbol{\phi} + \varepsilon_h(\dot{\tilde{\mathbf{U}}}, \boldsymbol{\phi}) + \int_\Gamma \left(1 - \frac{1}{\delta_h^\ell}\right)\dot{\mathbf{u}} : \boldsymbol{\phi}^\ell. \end{aligned} \tag{4.38}$$

In (4.38) we choose $\boldsymbol{\phi} = \boldsymbol{\theta}$. For the first term of (4.38), we observe that

$$\int_{\Gamma_h} I_h(\dot{\boldsymbol{\theta}} : \boldsymbol{\theta}) = \frac{1}{2}\frac{\mathrm{d}}{\mathrm{d}t}\|\boldsymbol{\theta}\|_h^2. \tag{4.39}$$

We estimate the single terms on the right-hand side of (4.38) in turn. By using the Cauchy–Schwarz inequality, the Lipschitz continuity of $\mathbf{f}$, the definition of $\boldsymbol{\theta}$, the relationships (4.2), (4.5) and (4.36), we have

$$\begin{aligned}\left|\int_{\Gamma_h} I_h((\mathbf{f}(\mathbf{U}) - \mathbf{f}(\mathbf{u}^{-\ell})) : \boldsymbol{\theta})\right| &\le \|\mathbf{f}(\mathbf{U}) - \mathbf{f}(\mathbf{u}^{-\ell})\|_h\|\boldsymbol{\theta}\|_h \le C\|\mathbf{U} - \mathbf{u}^{-\ell}\|_h\|\boldsymbol{\theta}\|_h \\ &\le C\left(\|\boldsymbol{\rho}\|_{L^2(\Gamma)} + \|\boldsymbol{\theta}\|_h\right)\|\boldsymbol{\theta}\|_h = C(\mathbf{u})\left(h^2 + \|\boldsymbol{\theta}\|_h\right)\|\boldsymbol{\theta}\|_h. \end{aligned} \tag{4.40}$$

By using estimate (4.4) for ε_h, (4.8), the regularity assumptions $\mathbf{f} \in \mathcal{C}^2(\Sigma)$ and $\mathbf{u} \in L^\infty([0,T], H^2(\Gamma))$ and by applying the chain rule to the composite function $\mathbf{f}(\mathbf{u})$, it follows that

$$\begin{aligned}\left|\varepsilon_h(\mathbf{f}(\mathbf{u}^{-\ell}), \boldsymbol{\theta})\right| &\le Ch^2\|\mathbf{f}(\mathbf{u}^{-\ell})\|_{H_h^2(\Gamma_h)}\|\boldsymbol{\theta}\|_{H^1(\Gamma_h)} \le C(1+h)h^2\|\mathbf{f}(\mathbf{u})\|_{H^2(\Gamma)}\|\boldsymbol{\theta}\|_{H^1(\Gamma_h)} \\ &\le C(h^2 + h^3)\|\mathbf{f}\|_{\mathcal{C}^2(\Sigma)}\|\mathbf{u}\|_{H^2(\Gamma)}\|\boldsymbol{\theta}\|_{H^1(\Gamma)} \le C(h^2 + h^3)\|\boldsymbol{\theta}\|_{H^1(\Gamma_h)}. \end{aligned} \tag{4.41}$$

Since $\mathbf{f}$ is Lipschitz over the compact region Σ, then $\mathbf{f} \in L^\infty(\Sigma)$. Hence, by using the Cauchy–Schwarz inequality and the geometric estimate (4.13), we have

$$\left|\int_\Gamma \left(1 - \frac{1}{\delta_h^\ell}\right)\mathbf{f}(\mathbf{u}) : \boldsymbol{\theta}\right| \le \left\|1 - \frac{1}{\delta_h^\ell}\right\|_{L^\infty(\Gamma)}\|\mathbf{f}(\mathbf{u})\|_{L^2(\Gamma)}\|\boldsymbol{\theta}\|_{L^2(\Gamma)} \le Ch^2\|\boldsymbol{\theta}\|_{L^2(\Gamma)}. \tag{4.42}$$

From the Cauchy–Schwarz inequality, the error estimate (4.37) and the inequality in (4.5) we have

$$\left|\int_{\Gamma_h} \dot{\boldsymbol{\rho}} : \boldsymbol{\theta}\right| \le C\|\dot{\boldsymbol{\rho}}\|_{L^2(\Gamma_h)}\|\boldsymbol{\theta}\|_{L^2(\Gamma_h)} \le C(\mathbf{u})h^2\|\boldsymbol{\theta}\|_{L^2(\Gamma_h)}. \tag{4.43}$$

From the estimate (4.4) for ε_h, the estimate (4.37) for $\boldsymbol{\rho}$, (4.5), (4.6) and the triangle inequality, we have

$$\begin{aligned}\left|\varepsilon_h(\dot{\tilde{\mathbf{U}}}, \boldsymbol{\theta})\right| &\le Ch^2\|\dot{\tilde{\mathbf{U}}}\|_{H^1(\Gamma_h)}\|\boldsymbol{\theta}\|_{H^1(\Gamma_h)} \le Ch^2\left(\|\dot{\boldsymbol{\rho}}\|_{H^1(\Gamma_h)} + \|\dot{\mathbf{u}}^{-\ell}\|_{H^1(\Gamma_h)}\right)\|\boldsymbol{\theta}\|_{H^1(\Gamma_h)} \\ &\le Ch^2\left(C(\mathbf{u})h + C\|\dot{\mathbf{u}}\|_{H^1(\Gamma)}\right)\|\boldsymbol{\theta}\|_{H^1(\Gamma_h)} \le C(\mathbf{u})(h^2 + h^3)\|\boldsymbol{\theta}\|_{H^1(\Gamma_h)}. \end{aligned} \tag{4.44}$$

We remark that, since for all $t \in [0,T]$, $\dot{\tilde{\mathbf{U}}}(\cdot,t) \in S_h$ is a piecewise linear function, we have $\dot{\tilde{\mathbf{U}}} : [0,T] \to H_h^2(\Gamma_h)$ and $\left|\dot{\tilde{\mathbf{U}}}(\cdot,t)\right|_{H_h^2(\Gamma_h)} = 0$ for all $t \in [0,T]$, where $|\cdot|_{H_h^2(\Gamma_h)}$ is the broken seminorm defined in (4.3). Hence, we have $\|\dot{\tilde{\mathbf{U}}}(\cdot,t)\|_{H_h^2(\Gamma_h)} = \|\dot{\tilde{\mathbf{U}}}(\cdot,t)\|_{H^1(\Gamma_h)}$, where $\|\cdot\|_{H^2(\Gamma_h)}$ is the broken Sobolev norm defined in (4.3). The Cauchy–Schwarz inequality, (4.5), the geometric estimate (4.13) and the stability bound (4.19) yield

$$\left|\int_\Gamma \left(1 - \frac{1}{\delta_h^\ell}\right) \dot{\mathbf{u}} : \boldsymbol{\theta}^\ell \right| \leq \left\| 1 - \frac{1}{\delta_h^\ell} \right\|_{L^\infty(\Gamma)} \|\dot{\mathbf{u}}\|_{L^2(\Gamma)} \|\boldsymbol{\theta}\|_{L^2(\Gamma_h)} \leq C(\mathbf{u}) h^2 \|\boldsymbol{\theta}\|_{L^2(\Gamma_h)}. \tag{4.45}$$

Combining (4.38)–(4.45), using (4.2), (4.5) and (4.6), we have

$$\begin{aligned} \frac{1}{2}\frac{\mathrm{d}}{\mathrm{d}t}\|\boldsymbol{\theta}\|_h^2 + m\|\nabla_{\Gamma_h}\boldsymbol{\theta}\|_{L^2(\Gamma_h)} &\leq C(\mathbf{u})\left(h^2 + h^3 + \|\boldsymbol{\theta}\|_h\right)\|\boldsymbol{\theta}\|_{H^1(\Gamma_h)} \\ &\leq C(\mathbf{u}, m)\left(h^4 + h^6 + \|\boldsymbol{\theta}\|_h^2\right) + m\|\boldsymbol{\theta}\|_{H^1(\Gamma_h)}^2, \end{aligned} \tag{4.46}$$

where $m = \min_{k=1,\ldots,r}\{d_k\}$. Cancelling $m\|\nabla_{\Gamma_h}\boldsymbol{\theta}\|_{L^2(\Gamma_h)}$ on both sides of (4.46), and again using (4.2), we have

$$\frac{\mathrm{d}}{\mathrm{d}t}\|\boldsymbol{\theta}\|_h^2 \leq C(\mathbf{u})(h^4 + h^6) + C(\mathbf{u})\|\boldsymbol{\theta}\|_h^2.$$

Using Grönwall's lemma, the assumption $\|\boldsymbol{\theta}_0^\ell\|_{L^2(\Gamma)} \leq Ch^2$, the norm estimates in (4.2) and (4.5), we obtain $\|\boldsymbol{\theta}^\ell\|_{L^2(\Gamma)}^2 \leq C(\mathbf{u}, T)(h^4 + h^6)$, which yields the desired result. □

In a similar fashion, following the approach in Nie & Thomée (1985) and Lakkis *et al.* (2013), we obtain the following $L^\infty([0,T], L^2(\Gamma))$ error estimate for the fully discrete solution (3.8).

THEOREM 4.9 (Error estimate for the fully discrete solution (3.8)) Assume that Σ is an invariant region for (3.3) and (3.8), that $\mathbf{f} \in \mathcal{C}^2(\Sigma)$ and that $\mathbf{u}_0, \mathbf{U}_0 \in \Sigma$. If the solution $\mathbf{u}$ of (3.3) and its time derivative $\dot{\mathbf{u}}$ are $L^\infty([0,T]; H^2(\Gamma))$, $\ddot{\mathbf{u}}$ is $L^\infty([0,T]; L^2(\Gamma))$ and $\left\|\mathbf{u}_0 - \mathbf{U}_0^\ell\right\|_{L^2(\Gamma)} \leq ch^2$ then the following estimate holds:

$$\|\mathbf{u}^n - \mathbf{U}^{\ell,n}\|_{L^2(\Gamma)} \leq C(\mathbf{u}, T)(h^2 + h^3 + \tau), \tag{4.47}$$

where $\mathbf{u}^n$ is the exact solution at time $t_n := n\tau$ and $C(\mathbf{u}, T)$ is a constant depending on $\mathbf{u}$ and T.

Proof. Let us write the error as

$$\mathbf{U}^{\ell,n} - \mathbf{u}^n = \left(\mathbf{U}^{\ell,n} - \bar{\mathbf{U}}^{\ell,n}\right) + \left(\bar{\mathbf{U}}^{\ell,n} - \mathbf{u}^n\right) =: \boldsymbol{\theta}^{\ell,n} + \boldsymbol{\rho}^{\ell,n} \quad \forall\, n, \tag{4.48}$$

and the discrete time derivative of any function $\boldsymbol{\phi} : \Gamma_h \times [0,T] \to \mathbb{R}^r$ as

$$\bar{\partial}\boldsymbol{\phi}^n := \frac{\boldsymbol{\phi}^n - \boldsymbol{\phi}^{n-1}}{\tau} \quad \forall\, n.$$

Since $\mathbf{u}$ and $\dot{\mathbf{u}}$ are $L^\infty([0,T],H^2(\Gamma))$, from (4.5), (4.6), (4.32) and (4.33), we have

$$\|\boldsymbol{\rho}^n\|_{L^2(\Gamma_h)} \le C\|\boldsymbol{\rho}^{\ell,n}\|_{L^2(\Gamma)} = \|\bar{\mathbf{U}}^{\ell,n} - \mathbf{u}^n\|_{L^2(\Gamma)} \le ch^2\|\mathbf{u}^n\|_{H^2(\Gamma)} \quad \forall\, n, \tag{4.49}$$

$$\|\dot{\boldsymbol{\rho}}^n\|_{L^2(\Gamma_h)} + h\|\nabla_{\Gamma_h}\dot{\boldsymbol{\rho}}^n\|_{L^2(\Gamma_h)} \le ch^2(\|\mathbf{u}^n\|_{H^2(\Gamma)} + \|\dot{\mathbf{u}}^n\|_{H^2(\Gamma)}) \quad \forall\, n. \tag{4.50}$$

It remains to show convergence for $\boldsymbol{\theta}^{\ell,n}$ in (4.48). To this end, we derive an estimate for $\boldsymbol{\theta}^n$ in the $L^2(\Gamma_h)$ norm and then use (4.2) and (4.5) to estimate $\|\boldsymbol{\theta}^{\ell,n}\|_{L^2(\Gamma)}$.

The continuous problem (3.3) and the fully discrete formulation (3.8), the definition of Ritz projection (4.31) and the relations (4.11), (4.12) imply that

$$\begin{aligned}
\int_{\Gamma_h} I_h(\bar\partial\boldsymbol{\theta}^n : \boldsymbol{\phi}^n) + \int_{\Gamma_h} D\nabla_{\Gamma_h}\boldsymbol{\theta}^n : \nabla_{\Gamma_h}\boldsymbol{\phi}^n &= -\varepsilon_h\left(\mathbf{f}\left(\mathbf{u}^{-\ell,n-1}\right),\boldsymbol{\phi}^n\right)\\
&+ \int_{\Gamma_h} I_h\left(\left(\mathbf{f}(\mathbf{U}^{n-1}\right) - \mathbf{f}\left(\mathbf{u}^{-\ell,n-1}\right)\right) : \boldsymbol{\phi}^n) - \int_\Gamma \left(1 - \frac{1}{\delta_h^\ell}\right)\mathbf{f}(\mathbf{u}^{n-1}) : \boldsymbol{\phi}^{\ell,n}\\
&+ \int_\Gamma \left(\mathbf{f}\left(\mathbf{u}^{n-1}\right) - \mathbf{f}(\mathbf{u}^n)\right) : \boldsymbol{\phi}^{\ell,n} - \int_{\Gamma_h} \bar\partial\boldsymbol{\rho}^n : \boldsymbol{\phi}^n + \varepsilon_h(\bar\partial\bar{\mathbf{U}}^n, \boldsymbol{\phi}^n)\\
&- \int_{\Gamma_h} (\bar\partial - \partial_t)\mathbf{u}^{-\ell,n} : \boldsymbol{\phi}^n + \int_\Gamma \left(1 - \frac{1}{\delta_h^\ell}\right)\dot{\mathbf{u}}^n : \boldsymbol{\phi}^{\ell,n}.
\end{aligned} \tag{4.51}$$

In (4.51), we choose $\boldsymbol{\phi}^n = \boldsymbol{\theta}^n$. For the first term in (4.51), from Young's inequality we have that

$$\int_{\Gamma_h} I_h\left(\bar\partial\boldsymbol{\theta}^n : \boldsymbol{\theta}^n\right) \ge \frac{1}{2\tau}\left(\|\boldsymbol{\theta}^n\|_h^2 - \|\boldsymbol{\theta}^{n-1}\|_h^2\right). \tag{4.52}$$

We estimate the single terms on the right-hand side of (4.51) in turn. From the Cauchy–Schwarz inequality, the Lipschitz continuity of $\mathbf{f}$, the definition of $\boldsymbol{\theta}^n$, (4.2) and (4.49), it follows that

$$\begin{aligned}
\left|\int_{\Gamma_h} I_h((\mathbf{f}(\mathbf{U}^{n-1}) - \mathbf{f}(\mathbf{u}^{-\ell,n-1})) : \boldsymbol{\theta}^n)\right| &\le \|\mathbf{f}(\mathbf{U}^{n-1}) - \mathbf{f}(\mathbf{u}^{-\ell,n-1})\|_h\|\boldsymbol{\theta}^n\|_h\\
&\le C\|\mathbf{U}^{n-1} - \mathbf{u}^{-\ell,n-1}\|_h\|\boldsymbol{\theta}^n\|_h \le C(\|\boldsymbol{\rho}^{n-1}\|_{L^2(\Gamma)} + \|\boldsymbol{\theta}^{n-1}\|_h)\|\boldsymbol{\theta}^n\|_h\\
&\le C(\mathbf{u})(h^2 + \|\boldsymbol{\theta}^{n-1}\|_h)\|\boldsymbol{\theta}^n\|_h.
\end{aligned} \tag{4.53}$$

From the estimate (4.4) for ε_h and (4.8), we obtain

$$\begin{aligned}
\left|\varepsilon_h(\mathbf{f}(\mathbf{u}^{-\ell,n-1}),\boldsymbol{\theta}^n)\right| &\le Ch^2\|\mathbf{f}(\mathbf{u}^{-\ell,n-1})\|_{H_h^2(\Gamma_h)}\|\boldsymbol{\theta}^n\|_{H^1(\Gamma_h)}\\
&\le C(1+h)h^2\|\mathbf{f}(\mathbf{u}^{n-1})\|_{H^2(\Gamma)}\|\boldsymbol{\theta}^n\|_{H^1(\Gamma_h)} \le C(1+h)h^2\|\mathbf{f}\|_{\mathcal{C}^2(\Sigma)}\|\mathbf{u}^{n-1}\|_{H^2(\Gamma)}\|\boldsymbol{\theta}^n\|_{H^1(\Gamma_h)}\\
&\le C(h^2+h^3)\|\boldsymbol{\theta}^n\|_{H^1(\Gamma_h)},
\end{aligned} \tag{4.54}$$

where we have exploited the regularity assumptions $\mathbf{f} \in \mathcal{C}^2(\Sigma)$ and $\mathbf{u} \in L^\infty([0,T],H^2(\Gamma))$. Since $\mathbf{f}$ is Lipschitz over the compact region Σ then $\mathbf{f} \in L^\infty(\Sigma)$. This fact, together with the Cauchy–Schwarz inequality, (4.5) and the geometric estimate (4.13) yields

$$\left|\int_\Gamma \left(1 - \frac{1}{\delta_h^\ell}\right)\mathbf{f}(\mathbf{u}^{n-1}) : \boldsymbol{\theta}^{\ell,n}\right| \le \left\|1 - \frac{1}{\delta_h^\ell}\right\|_{L^\infty(\Gamma)} \|\mathbf{f}(\mathbf{u}^{n-1})\|_{L^2(\Gamma_h)}\|\boldsymbol{\theta}^n\|_{L^2(\Gamma)} \le Ch^2\|\boldsymbol{\theta}^n\|_{L^2(\Gamma_h)}. \tag{4.55}$$

The Cauchy–Schwarz inequality, together with (4.5) and the stability estimate (4.20), yield

$$\begin{aligned}\left|\int_{\Gamma}(\mathbf{f}(\mathbf{u}^{n-1})-\mathbf{f}(\mathbf{u}^{n}))\cdot\boldsymbol{\theta}^{\ell,n}\right| &\leq \left\|\mathbf{f}\left(\mathbf{u}^{n-1}\right)-\mathbf{f}(\mathbf{u}^{n})\right\|_{L^2(\Gamma)}\|\boldsymbol{\theta}^{n}\|_{L^2(\Gamma_h)}\\ &\leq C\|\mathbf{u}^{n}-\mathbf{u}^{n-1}\|_{L^2(\Gamma)}\|\boldsymbol{\theta}^{n}\|_{L^2(\Gamma_h)}=\left\|\int_{t_{n-1}}^{t_n}\dot{\mathbf{u}}\right\|_{L^2(\Gamma)}\|\boldsymbol{\theta}^{n}\|_{L^2(\Gamma_h)}\\ &\leq \|\boldsymbol{\theta}^{n}\|_{L^2(\Gamma_h)}\int_{t_{n-1}}^{t_n}\|\dot{\mathbf{u}}\|_{L^2(\Gamma)}\leq\tau\|\dot{\mathbf{u}}\|_{L^\infty([0,T],L^2(\Gamma))}\|\boldsymbol{\theta}^{n}\|_{L^2(\Gamma_h)}=C(\mathbf{u})\tau\|\boldsymbol{\theta}^{n}\|_{L^2(\Gamma_h)}.\end{aligned}\tag{4.56}$$

From the Cauchy–Schwarz inequality and estimate (4.50) for $\dot{\boldsymbol{\rho}}$, we have

$$\begin{aligned}\left|\int_{\Gamma_h}\bar{\partial}\boldsymbol{\rho}^{n}:\boldsymbol{\theta}^{n}\right| &\leq C\|\bar{\partial}\boldsymbol{\rho}^{n}\|_{L^2(\Gamma_h)}\|\boldsymbol{\theta}^{n}\|_{L^2(\Gamma_h)}=\frac{C}{\tau}\left\|\int_{t_{n-1}}^{t_n}\dot{\boldsymbol{\rho}}\right\|_{L^2(\Gamma_h)}\|\boldsymbol{\theta}^{n}\|_{L^2(\Gamma_h)}\\ &\leq\frac{C}{\tau}\|\boldsymbol{\theta}^{n}\|_{L^2(\Gamma_h)}\int_{t_{n-1}}^{t_n}\|\dot{\boldsymbol{\rho}}\|_{L^2(\Gamma_h)}\leq C\|\dot{\boldsymbol{\rho}}\|_{L^\infty([0,T],L^2(\Gamma_h))}\|\boldsymbol{\theta}^{n}\|_{L^2(\Gamma_h)}\leq C(\mathbf{u})h^2\|\boldsymbol{\theta}^{n}\|_{L^2(\Gamma_h)}.\end{aligned}\tag{4.57}$$

From estimate (4.4) for ε_h, estimate (4.50) for $\boldsymbol{\rho}$, the equivalences (4.5), (4.6) and the triangle inequality, we obtain

$$\begin{aligned}\left|\varepsilon_h(\bar{\partial}\bar{\mathbf{U}}^{n},\boldsymbol{\theta}^{n})\right| &\leq Ch^2\|\bar{\partial}\bar{\mathbf{U}}^{n}\|_{H^1(\Gamma_h)}\|\boldsymbol{\theta}^{n}\|_{H^1(\Gamma_h)}\leq\frac{Ch^2}{\tau}\|\boldsymbol{\theta}^{n}\|_{H^1(\Gamma_h)}\int_{t_{n-1}}^{t_n}\|\dot{\tilde{\mathbf{U}}}\|_{H^1(\Gamma_h)}\\ &\leq Ch^2\|\dot{\tilde{\mathbf{U}}}\|_{L^\infty([0,T],H^1(\Gamma_h))}\|\boldsymbol{\theta}^{n}\|_{H^1(\Gamma_h)}\leq Ch^2\left(\|\dot{\boldsymbol{\rho}}\|_{L^\infty([0,T],H^1(\Gamma_h))}+\|\dot{\mathbf{u}}^{-\ell}\|_{L^\infty([0,T],H^1(\Gamma_h))}\right)\|\boldsymbol{\theta}^{n}\|_{H^1(\Gamma_h)}\\ &\leq Ch^2\left(C(\mathbf{u})h+C\|\dot{\mathbf{u}}\|_{L^\infty([0,T],H^1(\Gamma))}\right)\|\boldsymbol{\theta}^{n}\|_{H^1(\Gamma_h)}\leq C(\mathbf{u})(h^2+h^3)\|\boldsymbol{\theta}^{n}\|_{H^1(\Gamma_h)},\end{aligned}\tag{4.58}$$

where, for $\bar{\mathbf{U}}^{n}$, we have used the same argument explained after (4.44). From the Cauchy–Schwarz inequality and (4.5) we have

$$\begin{aligned}\left|\int_{\Gamma_h}(\bar{\partial}-\partial_t)\mathbf{u}^{-\ell,n}:\boldsymbol{\theta}^{n}\right| &\leq C\|(\bar{\partial}-\partial_t)\mathbf{u}^{n}\|_{L^2(\Gamma)}\|\boldsymbol{\theta}^{n}\|_{L^2(\Gamma_h)}\\ &\leq\frac{C}{\tau}\|\boldsymbol{\theta}^{n}\|_{L^2(\Gamma_h)}\int_{t_{n-1}}^{t_n}\|\dot{\mathbf{u}}(t)-\dot{\mathbf{u}}(t_n)\|_{L^2(\Gamma)}\mathrm{d}t\leq\frac{C}{\tau}\|\boldsymbol{\theta}^{n}\|_{L^2(\Gamma_h)}\int_{t_{n-1}}^{t_n}\int_{t}^{t_n}\|\ddot{\mathbf{u}}(s)\|\,\mathrm{d}s\,\mathrm{d}t\\ &\leq C\tau\|\ddot{\mathbf{u}}\|_{L^\infty([0,T],L^2(\Gamma))}\|\boldsymbol{\theta}^{n}\|_{L^2(\Gamma_h)}=C(\mathbf{u})\tau\|\boldsymbol{\theta}^{n}\|_{L^2(\Gamma_h)},\end{aligned}\tag{4.59}$$

where we have exploited the assumption that $\ddot{\mathbf{u}}\in L^\infty([0,T],L^2(\Gamma))$. The Cauchy–Schwarz inequality, (4.5), the geometric estimate (4.13) and the stability bound (4.19) yield

$$\left|\int_{\Gamma}\left(1-\frac{1}{\delta_h^{\ell}}\right)\dot{\mathbf{u}}^{n}:\boldsymbol{\theta}^{\ell,n}\right|\leq\left\|1-\frac{1}{\delta_h^{\ell}}\right\|_{L^\infty(\Gamma)}\|\dot{\mathbf{u}}^{n}\|_{L^2(\Gamma)}\|\boldsymbol{\theta}^{n}\|_{L^2(\Gamma_h)}\leq C(\mathbf{u})h^2\|\boldsymbol{\theta}^{n}\|_{L^2(\Gamma_h)}.\tag{4.60}$$

Combining (4.51)–(4.60), using (4.2) and Young's inequality we get

$$\frac{1}{2\tau}\left(\left\|\boldsymbol{\theta}^n\right\|_h^2-\left\|\boldsymbol{\theta}^{n-1}\right\|_h^2\right)+m\left\|\nabla_{\Gamma_h}\boldsymbol{\theta}^n\right\|_{L^2(\Gamma_h)}\leq C(\mathbf{u})\left(h^2+h^3+\tau+\left\|\boldsymbol{\theta}^{n-1}\right\|_h\right)\|\boldsymbol{\theta}^n\|_{H^1(\Gamma_h)}$$
$$\leq C(\mathbf{u},m)\left(h^4+h^6+\tau^2+\|\boldsymbol{\theta}^{n-1}\|_h^2\right)+m\|\boldsymbol{\theta}^n\|_{H^1(\Gamma_h)}^2, \tag{4.61}$$

where $m=\min_{k=1,\dots,r}\{d_k\}$, from which, cancelling $\|\nabla_{\Gamma_h}\boldsymbol{\theta}^{-\ell,n}\|_{L^2(\Gamma_h)}$ on both sides of (4.61), and using (4.2), we have

$$\left\|\boldsymbol{\theta}^n\right\|_h^2\leq(1+C(\mathbf{u})\tau)\left\|\boldsymbol{\theta}^{n-1}\right\|_h^2+C(\mathbf{u})\tau(h^4+h^6+\tau^2). \tag{4.62}$$

By repeatedly applying (4.62), taking into account the assumption that $\|\boldsymbol{\theta}^0\|_{L^2(\Gamma)}\leq Ch^2$, and then using (4.2), (4.5), we obtain

$$\left\|\boldsymbol{\theta}^{\ell,n}\right\|_{L^2(\Gamma)}^2\leq C(\mathbf{u})\left(h^4+h^6+\tau^2\right),$$

which yields the desired result. □

The previous theorems imply that our semidiscrete and fully discrete methods exhibit optimal convergence rates, that are quadratic in the meshsize h and linear in the timestep τ.

5. Numerical experiments

In this section, we provide numerical validation of our theoretical results and we show that the LSFEM combined with the IMEX Euler in time

- exhibits the optimal convergence rate predicted in Theorem 4.9 (see Sections 5.1–5.4);
- fulfils the discrete maximum principle for the homogeneous heat equation, while the standard SFEM does not (see Section 5.2);
- preserves the invariant rectangles of RDSs, while the standard SFEM does not (see Section 5.3).

The simulations have been carried out using MATLAB. In particular, the meshes for our numerical examples have been constructed by using the MATLAB package DistMesh (see Persson & Strang, 2004). *A posteriori*, we have verified that the generated meshes fulfil the Delaunay condition (2.11). The linear systems arising at each timestep have been solved with the MATLAB direct solver in the 'backslash' command. The code is available on request.

5.1 *Numerical experiment* 1: *the linear heat equation and convergence study*

In this experiment, we solve the parabolic equation (2.2) in the linear case $\alpha=1$ on the unit sphere $\Gamma=\{(x,y,z)\in\mathbb{R}^3|x^2+y^2+z^2=1\}$, given by

$$\begin{cases}\dot{u}-d\Delta_\Gamma u=-\beta u,\\ u_0(x,y,z)=xyz, \qquad (x,y,z)\in\Gamma,\end{cases} \tag{5.1}$$

TABLE 1 *Numerical experiment 1: comparisons of the convergence analysis in* $L^\infty([0,T],L^2(\Gamma_h))$ *norm between the SFEM and the LSFEM for the linear heat equation* (5.1) *with* $d = \frac{1}{24}$ *and* $\beta = \frac{1}{2}$.

			SFEM		LSFEM	
i	N	h	$L^\infty(L^2)$ error	Rate	$L^\infty(L^2)$ error	Rate
0	126	4.013e−01	6.100e−03	—	3.061e−03	—
1	258	2.863e−01	3.129e−03	1.977	1.846e−03	1.498
2	516	2.026e−01	1.594e−03	1.951	1.095e−03	1.510
3	1062	1.414e−01	7.899e−04	1.953	5.444e−04	1.945
4	2094	1.007e−01	3.966e−04	2.030	3.025e−04	1.731
5	4242	7.082e−02	2.013e−04	1.925	1.401e−04	2.184
6	8370	5.041e−02	1.003e−04	2.049	7.671e−05	1.773
7	16962	3.542e−02	5.063e−05	1.938	3.529e−05	2.200

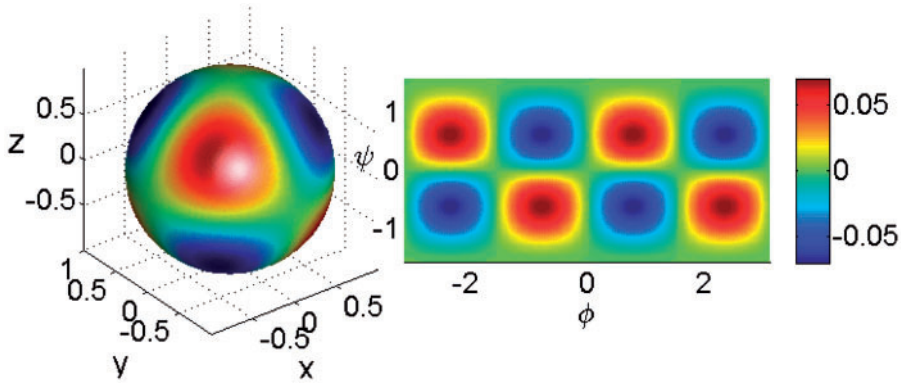

FIG. 2. *Numerical experiment 1*: The LSFEM solution corresponding to the linear heat equation (5.1) with $d = \frac{1}{24}$ and $\beta = \frac{1}{2}$ obtained on the Delaunay mesh for $i = 7$ with $N = 16962$ nodes, meshsize $h_7 = 3.542\text{e}{-2}$ and timestep $\tau_7 = 1.6\text{e}{-3}$ at $T = 1$ (left) and its planar projection through spherical coordinates (right).

with $d = \frac{1}{24}$ and $\beta = \frac{1}{2}$, to test the convergence rate of the LSFEM method. The exact solution of (5.1) is $u(x,y,z,t) = xyz\,e^{-t}$, $(x,y,z) \in \Gamma$, $t \geq 0$. In this experiment, as well as in the following examples, the problem is solved on a sequence of eight meshes Γ_i, $i = 0,\ldots,7$ with corresponding meshsizes h_i with $h_0 = 4.013\text{e-}1$ and $h_i \approx \sqrt{2}^{-i} h_0$ for all $i = 1,\ldots,7$ and corresponding timesteps τ_i with $\tau_0 = 0.2$ and $\tau_i = 2^{-i}\tau_0$ for all $i = 1,\ldots,7$ (see parameter values in Table 1). Hence, τ_i is approximately proportional to h_i^2 to reveal the quadratic convergence, with respect to the meshsize of the method. All of the τ_i fulfil the stability condition given in Theorem 2.4. For every $i = 0,\ldots,7$, the $L^\infty([0,T],L^2(\Gamma_h))$ error between the numerical solution U and the interpolant $I_h(u)$ of the exact solution is reported in Table 1. The lumped solution U at the final time $T = 1$ obtained on the finest mesh is shown in Fig. 2 (left), as well as its planar projection through spherical coordinates (right)

$$x = \cos\phi\cos\psi, \quad y = \cos\phi\sin\psi, \quad z = \sin\psi, \quad \text{with} \quad (\phi,\psi) \in [-\pi,\pi] \times \left[-\frac{\pi}{2},\frac{\pi}{2}\right].$$

In this example, the predicted second-order convergence in space is attained. Furthermore, we observe that, for this specific example, the lumped SFEM exhibits a better accuracy than the standard SFEM. We

TABLE 2 *Numerical experiment 2: discrete maximum principle analysis on* $\Gamma_h \times]0,T]$: *comparisons between the SFEM and the LSFEM for the homogeneous heat equation* (2.2) *with* $\beta = 0$ *and initial datum* (5.2).

i	N	h	$\min_{\Gamma_h \times [\tau,1]} U$ SFEM	$\min_{\Gamma_h \times [\tau,1]} U$ LSFEM
0	126	4.013e−01	−3.454e−04	7.016e−09
1	258	2.863e−01	−4.695e−06	4.812e−12
2	516	2.026e−01	−1.299e−03	1.213e−16
3	1062	1.414e−01	−2.123e−07	2.746e−23
4	2094	1.007e−01	−7.546e−04	3.142e−32
5	4242	7.082e−02	−1.037e−05	1.816e−45
6	8370	5.041e−02	−4.163e−04	5.324e−64
7	16962	3.542e−02	−1.254e−04	3.126e−90

believe that this phenomenon, which does not occur in general, is due to the particular symmetry of the considered problem.

5.2 *Numerical experiment 2: the homogeneous heat equation and the maximum principle*

We solve the parabolic equation (2.2) for the homogeneous case $\beta = 0$ on the unit sphere Γ with $d = 0.1$ until the final time $T = 1$ and the non-negative compactly supported $H^1(\Gamma)$ initial datum

$$u_0(x,y,z) = \begin{cases} \sqrt{1 - \frac{x^2+y^2}{0.04}} & \text{if } x^2 + y^2 \leq 0.04,\ z > 0, \\ 0 & \text{elsewhere.} \end{cases} \tag{5.2}$$

In this case, the invariant region is $\Sigma = [0,1]$, then the solution must stay non-negative at all times. Moreover, since $\beta = 0$, the IMEX Euler time discretization reduces to implicit Euler. The minima of the computed numerical solution obtained by SFEM and LSFEM for each mesh (h_i, τ_i), $i = 0, \ldots, 7$, (constructed as in the previous example, see Section 5.1), are reported in Table 2. This experiment confirms our findings, as the LSFEM fulfils the discrete maximum principle, while the standard SFEM violates the maximum principle as illustrated in Table 2.

5.3 *Numerical experiment 3: RDS and the preservation of the invariant rectangle*

In this experiment, we consider the RDS with Rosenzweig–MacArthur kinetics (see González-Olivares & Ramos-Jiliberto, 2003; Garvie & Trenchea, 2007)

$$\begin{cases} u_t - d_1 \Delta_\Gamma u = au(1-u) - b\frac{uv}{u+\alpha}, \\ v_t - d_2 \Delta_\Gamma v = c\frac{uv}{u+\alpha} - dv, \end{cases} \tag{5.3}$$

where α, a, b, c and d are positive constants, d_1 and d_2 are positive diffusion coefficients. The surface considered is the *Dupin ring cyclide* $\Gamma := \left\{(x,y,z) \in \mathbb{R}^3 : \left(x^2+y^2+z^2+\frac{261}{100}\right)^2 - 4\left(2x - \frac{\sqrt{39}}{10}\right)^2 - \frac{361}{25}y^2 = 0\right\}$ (see Fuselier & Wright, 2013).

This system has been numerically solved in Garvie & Trenchea (2007) on a planar domain with LFEM in combination with an implicit Euler time discretization. However, since the theory developed in Garvie & Trenchea (2007) addresses a problem on domains of more general dimension ($n \leq 3$), there is no discrete maximum principle and the authors consider modified kinetics to ensure the positivity of the numerical solution. The present example shows that, on two-dimensional manifolds, lumping guarantees the preservation of the invariant region without the need of modifying the kinetics.

When $c = d$ and $0 < \alpha < \frac{1}{\sqrt{2}}$ for every $0 < \varepsilon < 1 - 2\sqrt{a}$, the rectangle

$$\Sigma := [\varepsilon, 1] \times \left[0, \frac{a\alpha}{2b}\right] \tag{5.4}$$

is an invariant region for (5.3), see, for instance, the analysis in González-Olivares & Ramos-Jiliberto (2003). An easy way to see this is to observe that, for every $\varepsilon, \varepsilon' > 0$, the rectangle

$$\Sigma_1 := \left[\varepsilon, 1 + \frac{\varepsilon' a\alpha}{b}\right] \times \left[-\varepsilon', \frac{a\alpha}{2b}\right]$$

fulfils condition (3.11). Since the intersection of invariant regions is still invariant, then Σ is invariant for (5.3). The $H^1(\Gamma)$ initial datum

$$u_0(x, y, z) = \begin{cases} \varepsilon + (1 - \varepsilon)\sqrt{1 - \frac{y^2}{0.16}} & \text{if } y^2 \leq 0.16, \\ 0 & \text{elsewhere,} \end{cases}$$
$$v_0(x, y, z) = \frac{a\alpha}{2b} \qquad \forall\, (x, y, z) \in \Gamma,$$

is contained in the invariant region Σ. Furthermore, for $0 < \alpha < 1$, it is easy to verify that, in Σ, the Lipschitz constants L_1 and L_2 of the kinetics in (5.3) fulfil

$$L_1 < \sqrt{2}\left(3a + \frac{b}{2\alpha}\right) \quad \text{and} \quad L_2 < \sqrt{2}\left(\frac{c}{2\alpha} + \frac{d}{2}\right).$$

In the following, we choose $d_1 = d_2 = 1e\text{-}2$, $\alpha = 1e\text{-}3$, $a = 10$, $b = 1e\text{-}2$, $c = d = 1$ and $\varepsilon = 1e\text{-}7$. With these settings, the invariant region (5.4) becomes

$$\Sigma = [1e\text{-}7, 1] \times \left[0, \frac{1}{2}\right], \tag{5.5}$$

and the stability condition (3.18) on the timestep is fulfilled if we choose

$$\tau \leq \bar{\tau} := \frac{1}{\sqrt{2}\max\left\{\left(3a + \frac{b}{2\alpha}\right), \left(\frac{c}{2\alpha} + \frac{d}{2}\right)\right\}} = 1.4e\text{-}3. \tag{5.6}$$

We thus solve the problem on a sequence of seven spatial meshes Γ_i, $i = 0, \ldots, 6$ with corresponding meshsizes h_i with $h_0 = 1.190$ and $h_i \approx \sqrt{2}^{-i} h_0$ for all $i = 1, \ldots, 6$, with a fixed timestep $\bar{\tau} = 1e{-}3$ and final time $T = 5$. In Tables 3 and 4, we show the minima and the maxima of the components of the computed numerical solutions: we observe that the LSFEM solutions preserve Σ, while the SFEM ones

TABLE 3 *Numerical experiment 3: invariance analysis for the SFEM solutions of* (5.3) *with parameters and initial datum as reported in the main text. The solutions blow up on all meshes.*

i	N	h	$\min_{\Gamma_h\times[\tau,5]}$ U	$\max_{\Gamma_h\times[\tau,5]}$ U	$\min_{\Gamma_h\times[\tau,5]}$ V	$\max_{\Gamma_h\times[\tau,5]}$ V
0	242	1.190e+00	−2.199e+173	1.670e+169	−1.157e−01	5.159e−01
1	486	8.537e−01	−1.654e+161	2.663e+157	−1.629e+00	7.239e−01
2	986	5.898e−01	−2.788e+254	5.341e+250	−5.002e−01	2.170e+00
3	1950	4.273e−01	−4.164e+174	7.136e+170	−2.448e+00	3.394e+00
4	3866	3.011e−01	−5.784e+215	8.624e+211	−2.816e+00	7.301e+00
5	7766	2.114e−01	−1.961e+158	5.002e+154	−2.472e+01	2.114e+01
6	15552	1.531e−01	−2.891e+178	1.688e+175	−5.529e+01	1.085e+01

TABLE 4 *Numerical experiment 3: invariance analysis for the LSFEM solutions of* (5.3) *with parameters and initial datum as reported in the main text. The values of N and h are as in Table 3. The solutions stay in the invariant rectangle* $[1\mathrm{e}{-7}, 1] \times \left[0, \frac{1}{2}\right]$ *for all meshes. The minima of U coincide up to machine precision.*

i	$\min_{\Gamma_h\times[\tau,5]}$ U	$\max_{\Gamma_h\times[\tau,5]}$ U	$\min_{\Gamma_h\times[\tau,5]}$ V	$\max_{\Gamma_h\times[\tau,5]}$ V
0	1.005e−07	0.999919049314999	0.140403459482026	0.499999499006500
1	1.005e−07	0.999859791592458	0.140314932710790	0.499999500147031
2	1.005e−07	0.999928903829794	0.140311706814337	0.499999500464241
3	1.005e−07	0.999882762800890	0.140311624718897	0.499999500411808
4	1.005e−07	0.999929620790774	0.140311624053878	0.499999500465688
5	1.005e−07	0.999932927703920	0.140311624044096	0.499999500467816
6	1.005e−07	0.999934143729114	0.140311624043996	0.499999500468662

blow up on all meshes. In Fig. 3 we show, for the v component, the SFEM (left) and the LSFEM (right) solutions, computed on the mesh for $i = 6$, at the time $\bar{t} := 0.4770$ in which the SFEM solution attains its absolute minimum (-5.529). In Fig. 3, we set the bounds of the grayscale (colourmap online) to the end points of the invariant region ($[0, 0.5]$) to highlight the points on the surface in which the SFEM solution violates the region.

5.4 *Numerical experiment 4: RDS with activator-depleted kinetics and convergence study*

In this example, we test the convergence rate of the LSFEM method on the unit sphere Γ for the well-studied *activator-depleted* substrate kinetics (see Prigogine & Lefever, 1968; Gierer & Meinhardt, 1972; Schnakenberg, 1979; Murray, 2001) with an additional forcing term

$$\begin{cases} u_t - d_1 \Delta_\Gamma u = a - u + u^2 v + f_1(x, y, z, t), \\ v_t - d_2 \Delta_\Gamma v = b - u^2 v + f_2(x, y, z, t), \end{cases} \tag{5.7}$$

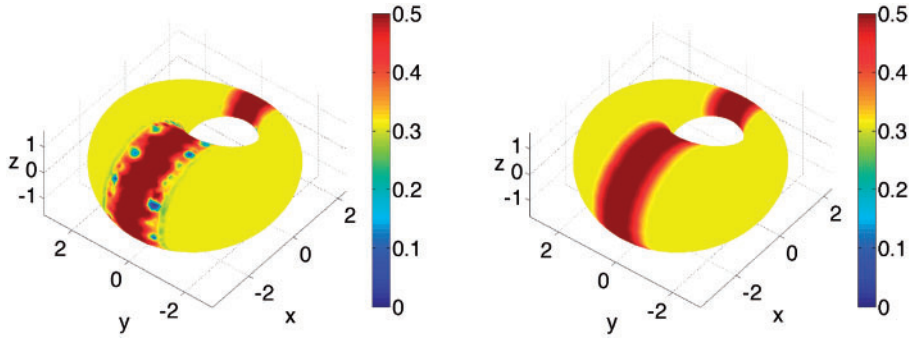

FIG. 3. Numerical experiment 3: component v of the numerical solution of (5.3) with $d_1 = d_2 = 1\text{e}{-2}$, $\alpha = 1\text{e}{-3}$, $a = 10$, $b = 1\text{e}{-2}$, $c = d = 1$ obtained on a mesh with $N = 15552$ grid points and $h = 0.1531$. Numerical solutions by the SFEM (left) and the LSFEM (right) at the time $\bar{t} = 0.477$. The bounds of the grayscale (colourmap online) are set to $[0, 0.5]$ to highlight the points in which the SFEM solution violates the invariant region (5.5).

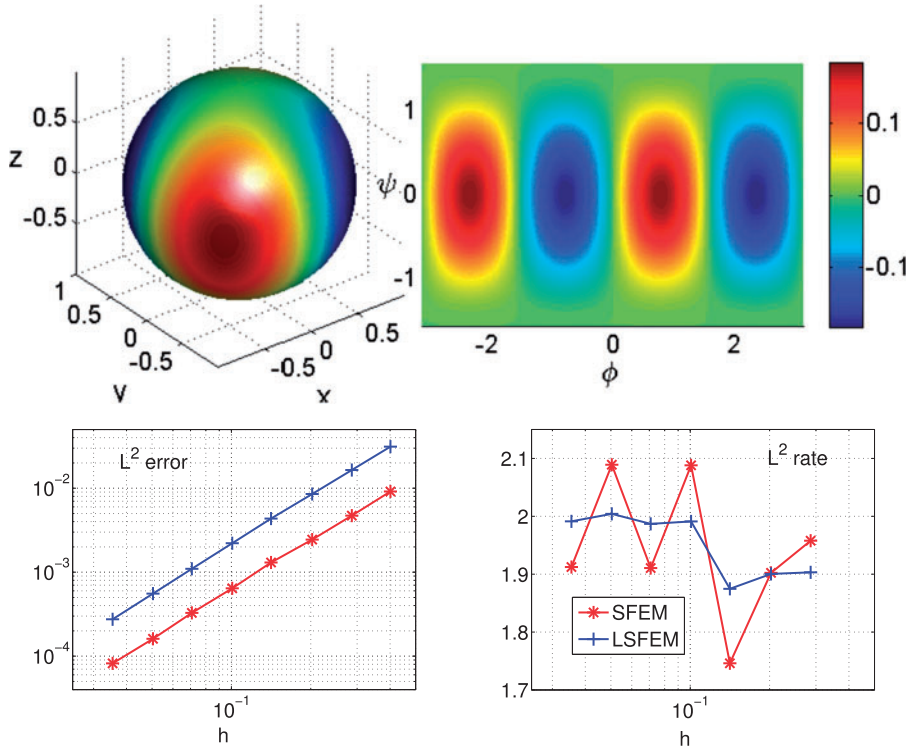

FIG. 4. Numerical experiment 4. Top row: the u-component of the LSFEM solution corresponding to the RDS with *activator-depleted* substrate kinetics (5.7) with $a = b = 1$, $d_1 = \frac{1}{6}$, $d_2 = \frac{1}{12}$ and initial condition as stated in the text, obtained on a mesh with $N = 16962$ nodes and timestep $\tau = 1.6\text{e}{-3}$ at $T = 1$ and their corresponding planar projections through spherical coordinates. Bottom row: convergence analysis of the SFEM and the LSFEM. As predicted, the LSFEM retains the quadratic convergence rate of SFEM.

where the functions $f_1(\mathbf{x}, t)$ and $f_2(\mathbf{x}, t)$ are chosen in such a way that the exact solution is known at all times. Although this example is beyond the scope of the present work, due to the space and time dependence of the reaction terms, we include it merely as a numerical test. We choose $a = b = 1$, $d_1 = \frac{1}{6}, d_2 = \frac{1}{12}, f_1(x, y, z, t) = xy\, e^{-t}(1 + x^2y^2\, e^{-2t}) - a, f_2(x, y, z, t) = -x^3y^3z\, e^{-t} - b$ and the following initial condition: $u_0(x, y, z) = xy$, and $v_0(x, y, z) = -xyz$ for all $(x, y, z) \in \Gamma$. In this case, the exact solution is given by $u(x, y, z, t) = xy\, e^{-t}$ and $v(x, y, z, t) = -xyz\, e^{-t}$ for all $(x, y, z) \in \Gamma$ and $t \geq 0$. We solve the problem on the same sequence of meshes and timesteps considered in numerical experiment 1, with final time $T = 1$, for both the SFEM and the LSFEM, where the contributions due to the forcing terms f_k, $k = 1, 2$ are approximated with the standard and lumped quadrature rules given by

$$\int_{\Gamma_h} I_h(f_k)\chi_i, \quad \text{and} \quad \int_{\Gamma_h} I_h(f_k\chi_i), \quad \forall\, i = 1, \ldots, N,$$

respectively. We observe that the standard quadrature rule is exact for piecewise linear functions, while the lumped one is only exact when the product of the functions is piecewise linear. For this reason, the LSFEM is expected to produce larger errors than the SFEM. The L^2 errors and experimental convergence rates are plotted in Fig. 4 together with the u component of the LSFEM solution obtained on the finest mesh at the final time $T = 1$. As expected, the LSFEM exhibits slightly larger errors than the SFEM. Nonetheless, they have the same convergence rate, in agreement with our theoretical findings.

6. Conclusions

The contributions of the present paper can be summarized as follows:

- In Section 2, we considered a class of semilinear parabolic scalar problems on surfaces. For the spatial discretization, we introduced introduced a lumped surface finite element method (LSFEM), by extending its planar counterpart in Nie & Thomée (1985), inspired by the ideas in Dziuk & Elliott (2013a). We carried out a time discretization by applying the IMEX Euler method. We showed in Theorem 2.3 that the spatially discrete problem fulfils a discrete maximum principle. In particular, we proved that no restriction on the timestep is required in the homogeneous case (thus extending the result of Thomée, 1984 to surfaces); the timestep restriction (2.29) is required in the presence of the nonlinear reaction term in (2.2).
- In Section 3, we applied the LSFEM space discretization and the IMEX Euler time discretization to general systems of arbitrarily many reaction–diffusion equations. In analogy with the continuous setting (see Chueh *et al.*, 1977), in Theorem 3.3 we showed that under the sole assumption of Delaunay regularity for the mesh, one of the two strictly inward flux conditions (3.13)–(3.16) is sufficient for a rectangle in the phase space to be invariant for the spatially discrete scheme. For the fully discrete problem, we showed in Theorem 3.5 that under the timestep restriction (3.18) involving the Lipschitz constants of the reaction kinetics, condition (3.11) is still not only sufficient to ensure a hyperrectangle is invariant but can even be weakened by requiring nonoutward fluxes (3.17). To the best of our knowledge, Theorems 3.3 and 3.5 are a novelty also on planar domains.
- For both the semidiscrete and fully discrete formulations of the RDSs considered in Section 3, including the parabolic problem of Section 2 as a special case, optimal $L^\infty([0, T], L^2(\Gamma))$ error bounds were proved in Section 4.
- The numerical examples in Section 5 confirm our theoretical findings. The usefulness of the LSFEM is illustrated in numerical experiments 2 and 3. In particular, we showed that in the absence of

lumping, the numerical solution of the homogeneous heat equation violates the maximum principle (Section 5.2) and the numerical solution of a classical predator–prey model blows up instead of being bounded by the invariant rectangle (numerical experiment 3).

Emerging applications encourage the extension of the present study to more general cases of RDSs, for example, where cross-diffusion is present and/or when the surface is evolving in time, which are beyond the scope of this work and will be addressed in future studies.

Acknowledgements

The authors (MF, AM, IS, CV) would like to thank the Isaac Newton Institute for Mathematical Sciences for its hospitality during the programme [Coupling Geometric PDEs with Physics for Cell Morphology, Motility and Pattern Formation]. AM acknowledges funding from the European Union Horizon 2020 research and innovation programme and AM is a Royal Society Wolfson Research Merit Award Holder funded generously by the Wolfson Foundation. IS's research work has been performed under the auspices of the Italian National Group for Scientific Calculus (GNCS-INdAM).

Funding

Engineering and Physical Sciences Research Council (EP/J016780/1 A.M., C.V. in part, EP/K032208/1 to A.M., C.V., I.S., C.V.); Leverhulme Trust Research Project Grant (RPG-2014-149); Marie Skłodowska-Curie (642866); and Simons Foundation to A.M., in part.

References

Alikakos, N. D. (1979) An application of the invariance principle to reaction–diffusion equations. *J. Differential Equations,* **33**, 201–225.

Barreira, M. R. (2009) Numerical solution of non-linear partial differential equations on triangulated surfaces. *Ph.D. Thesis*, University of Sussex.

Barreira, R., Elliott, C. M. & Madzvamuse, A. (2011) The surface finite element method for pattern formation on evolving biological surfaces. *J. Math. Biol.,* **63**, 1095–1119.

Becherer, D. & Schweizer, M. (2005) Classical solutions to reaction–diffusion systems for hedging problems with interacting Itô and point processes. *Ann. Appl. Probab.,* **15**, 1111–1144.

Bertalmío, M., Mémoli, F., Cheng, L.-T., Sapiro, G. & Osher, S. (2003) Variational problems and partial differential equations on implicit surfaces: bye bye triangulated surfaces? *Geometric Level Set Methods in Imaging, Vision, and Graphics.* New York: Springer-Verlag, pp. 381–397.

Bessler, W. G. (2005) A new computational approach for SOFC impedance from detailed electrochemical reaction–diffusion models. *Solid State Ionics*, **176**, 997–1011.

Burman, E., Claus, S., Hansbo, P., Larson, M. G. & Massing, A. (2015) Cutfem: discretizing geometry and partial differential equations. *Int. J. Numer. Methods Eng.,* **104**, 472–501.

Canuto, C., Hussaini, M. Y., Quarteroni, A. M., ZANG, T. A., Jr. (2012) *Spectral Methods in Fluid Dynamics*. Heidelberg, Berlin: Springer.

Chaplain, M. A. J., Ganesh, M. & Graham, I. G. (2001) Spatio-temporal pattern formation on spherical surfaces: numerical simulation and application to solid tumour growth. *J. Math. Biol.,* **42**, 387–423.

Chatzipantelidis, P., Horváth, Z. & Thomée, V. (2015) On preservation of positivity in some finite element methods for the heat equation. *Comput. Methods Appl. Math.,* **15**, 417–437.

Chellaboina, V., Bhat, S. P., Haddad, W. M. & Bernstein, D. S. (2009) Modeling and analysis of mass-action kinetics. *IEEE Control Syst.,* **29**, 60–78.

CHUEH, K. N., CONLEY, C. C. & SMOLLER, J. A. (1977) Positively invariant regions for systems of nonlinear diffusion equations. *Indiana Univ. Math. J.,* **26**, 373–392.

DASSI, F. (2014) Advanced techniques for the generation and the adaptation of complex surface meshes. *Ph.D. Thesis*, Politecnico di Milano.

DU, Q., JU, L. & TIAN, L. (2011) Finite element approximation of the Cahn–Hilliard equation on surfaces. *Comput. Methods Appl. Mech. Engrg.,* **200**, 2458–2470.

DYER, R. (2010) Self-Delaunay meshes for surfaces, *Ph.D. Thesis*, Simon Fraser University.

DZIUK, G. (1988) Finite elements for the Beltrami operator on arbitrary surfaces. *Calc. Var. Partial Differential Equations,* pp. 142–155.

DZIUK, G. & ELLIOTT, C. M. (2013a) Finite element methods for surface PDEs. *Acta Numer.,* **22**, 289–396.

DZIUK, G. & ELLIOTT, C. M. (2013b) L^2-estimates for the evolving surface finite element method. *Math. Comp.,* **82**, 1–24.

EILKS, C. & ELLIOTT, C. M. (2008) Numerical simulation of dealloying by surface dissolution via the evolving surface finite element method. *J. Comput. Phys.,* **227**, 9727–9741.

ELLIOTT, C. M. & RANNER, T. (2015) Evolving surface finite element method for the Cahn–Hilliard equation. *Numer. Math.*, **129**, 483–534.

ELLIOTT, C. M. & STINNER, B. (2010) Modeling and computation of two phase geometric biomembranes using surface finite elements. *J. Comput. Phys.,* **229**, 6585–6612.

ELLIOTT, C. M., STINNER, B. & VENKATARAMAN, C. (2012) Modelling cell motility and chemotaxis with evolving surface finite elements. *J. Roy. Soc. Interface,* 3027–3044.

ELLIOTT, C. M. & STUART, A. M. (1993) The global dynamics of discrete semilinear parabolic equations. *SIAM J. Numer. Anal.,* **30**, 1622–1663.

FARAGÓ, I., KARÁTSON, J. & KOROTOV, S. (2012) Discrete maximum principles for nonlinear parabolic PDE systems. *IMA J. Numer. Anal.,* **34**, 1541–1573.

FERREIRA JR, S. C., MARTINS, M. L. & VILELA, M. J. (2002) Reaction–diffusion model for the growth of avascular tumor. *Phys. Rev. E,* **65**, 021907.

FUSELIER, E. J. & WRIGHT, G. B. (2013) A high-order kernel method for diffusion and reaction–diffusion equations on surfaces. *J. Sci. Comput.,* **56**, 535–565.

GALUSINSKI, C. (1998) Existence and continuity of uniform exponential attractors of the singularity perturbed Hodgkin–Huxley system. *J. Differential Equations*, **144**, 99–169.

GARVIE, M. R. & TRENCHEA, C. (2007) Finite element approximation of spatially extended predator–prey interactions with the Holling type II functional response. *Numer. Math.,* **107**, 641–667.

GIERER, A. & MEINHARDT, H. (1972) A theory of biological pattern formation. *Kybernetika (Prague)*, **12**, 30–39.

GILBARG, D. & TRUDINGER, N. S. (2015) *Elliptic Partial Differential Equations of Second Order*. Heidelberg, Berlin: Springer.

GONZÁLEZ-OLIVARES, E. & RAMOS-JILIBERTO, R. (2003) Dynamic consequences of prey refuges in a simple model system: more prey, fewer predators and enhanced stability. *Ecol. Model.,* **166**, 135–146.

HEBEY, E. & ROBERT, F. (2008) Sobolev spaces on manifolds. *Handbook of Global Analysis.* Amsterdam: Elsevier, pp. 375–415.

HOFF, D. (1978) Stability and convergence of finite difference methods for systems of nonlinear reaction-diffusion equations. *SIAM J. Numer. Anal.,* **15**, 1161–1177.

KIM, J. & MOIN, P. (1985) Application of a fractional-step method to incompressible Navier–Stokes equations. *J. Comput. Phys.,* **59**, 308–323.

KOVÁCS, B., LI, B., LUBICH, C., & GUERRA, C. A. P. (2017) Convergence of finite elements on an evolving surface driven by diffusion on the surface. *Numerische Mathematik*, published online.

KOVÁCS, B. & LUBICH, C. (2016) Numerical analysis of parabolic problems with dynamic boundary conditions. *IMA J. Numer. Anal.,* **37**, 1–39.

KOVÁCS, S. (2003) Spatial inhomogeneity due to Turing bifurcation in a system of Gierer-Meinhardt type. *J. Appl. Math. Comput.,* **11**, 125–141.

LACITIGNOLA, D., BOZZINI, B., FRITTELLI, M. & SGURA, I. (2017) Turing pattern formation on the sphere for a morphochemical reaction–diffusion model for electrodeposition. *Commun. Nonlinear Sci. Numer. Simul.,* **48**, 484–508.

LACITIGNOLA, D., BOZZINI, B. & SGURA, I. (2015) Spatio-temporal organization in a morphochemical electrodeposition model: Hopf and Turing instabilities and their interplay. *European J. Appl. Math.,* **26**, 143–173.

LAKKIS, O., MADZVAMUSE, A. & VENKATARAMAN, C. (2013) Implicit–explicit timestepping with finite element approximation of reaction–diffusion systems on evolving domains. *SIAM J Numer. Anal.,* **51**, 2309–2330.

MACDONALD, C. B. (2008) The closest point method for time-dependent processes on surfaces, *Ph.D. Thesis*, Dept. of Mathematics-Simon Fraser University.

MACDONALD, C. B. & RUUTH, S. J. (2009) The implicit closest point method for the numerical solution of partial differential equations on surfaces. *SIAM J. Sci. Comput.,* **31**, 4330–4350.

MADZVAMUSE, A. (2006) Time-stepping schemes for moving grid finite elements applied to reaction–diffusion systems on fixed and growing domains. *J. Comput. Phys.,* **214**, 239–263.

MURRAY, J. D. (2001) *Mathematical Biology. II Spatial Models and Biomedical Applications*, New York: Springer.

NIE, Y.-Y. & THOMÉE, V. (1985) A lumped mass finite element method with quadrature for a non-linear parabolic problem. *IMA J. Numer. Anal.,* **5**, 371–396.

NIJHOUT, H. F., MAINI, P. K., MADZVAMUSE, A., WATHEN, A. J. & SEKIMURA, T. (2003) Pigmentation pattern formation in butterflies: experiments and models. *C. R. Biol.,* **326**, 717–727.

NOCHETTO, R. H. & VERDI, C. (1996) Combined effect of explicit time-stepping and quadrature for curvature driven flows. *Numer. Math.,* **74**, 105–136.

OLSHANSKII, M. A., REUSKEN, A. & GRANDE, J. (2009) A finite element method for elliptic equations on surfaces. *SIAM J. Numer. Anal.,* **47**, 3339–3358.

PERSSON, P.-O. (2004) Mesh generation for implicit geometries, *Ph.D. Thesis*, Massachusetts Institute of Technology.

PERSSON, P.-O. & STRANG, G. (2004) A simple mesh generator in MATLAB. *SIAM Rev.,* **46**, 329–345.

PRIGOGINE, I. & LEFEVER, R. (1968) Symmetry breaking instabilities in dissipative systems. II. *J. Chem. Phys.,* **48**, 1695–1700.

RAUCH, J. & SMOLLER, J. (1978) Qualitative theory of the FitzHugh–Nagumo equations. *Adv. Math.,* **27**, 12–44.

RAVIART, P.-A. (1973) The use of numerical integration in finite element methods for solving parabolic equations. *in Topics of Numerical Analysis*, New York: Academic Press, pp. 233–264.

RUUTH, S. J. (1995) Implicit-explicit methods for reaction–diffusion problems in pattern formation. *J. Math. Biol.,* **34**, 148–176.

SCHNAKENBERG, J. (1979) Simple chemical reaction systems with limit cycle behaviour. *J. Theoret. Biol.,* **81**, 389–400.

SHANKAR, V., WRIGHT, G. B., KIRBY, R. B. & FOGELSON, A. L. (2015) A radial basis function (RBF) —finite difference (FD) for diffusion and reaction–diffusion equations on surfaces. *J. Sci. Comput.,* **63**, 745–768.

SKALSKI, G. T. & GILLIAM, J. F. (2001) Functional responses with predator interference: viable alternatives to the Holling type II model. *Ecology,* **82**, 3083–3092.

SMOLLER, J. (1994) *Shock Waves and Reaction–Diffusion Equations.* New York: Springer.

TAYLOR, M. E. (1997) *Partial Differential Equations. III.* New York: Springer.

THOMÉE, V. (1984) *Galerkin Finite Element Methods for Parabolic Problems.* Berlin: Springer.

TUNCER, N., MADZVAMUSE, A. & MEIR, A. J. (2015) Projected finite elements for reaction–diffusion systems on stationary closed surfaces. *Appl. Numer. Math.,* **96**, 45–71.

VANAG, V. K. (2004) Waves and patterns in reaction–diffusion systems. Belousov–Zhabotinsky reaction in water-in-oil microemulsions. *Phys. Uspekhi,* **47**, 923–941.

VAREA, C., ARAGON, J. L. & BARRIO, R. A. (1999) Turing patterns on a sphere. *Phys. Rev. E,* **60**, 4588.

YOU, Y. (2012) Global dynamics of the Oregonator system. *Math. Methods Appl. Sci.,* **35**, 398–416.